

# COMPRESSED DATA STRUCTURES FOR HEEGAARD SPLITTINGS

HENRIQUE ENNES AND CLÉMENT MARIA

**ABSTRACT.** Heegaard splittings provide a natural representation of closed 3-manifolds by gluing handlebodies along a common surface. These splittings can be equivalently given by two finite sets of meridians lying in the surface, which define a Heegaard diagram. We present a data structure to effectively represent Heegaard diagrams as normal curves with respect to triangulations of a surface of complexity measured by the space required to express the normal coordinates' vectors in binary. This structure can be significantly more compressed than triangulations of 3-manifolds, given exponential gains for some families. Even with this succinct definition of complexity, we establish polynomial time algorithms for comparing and manipulating diagrams, performing stabilizations, detecting trivial stabilizations and reductions, and computing topological invariants of the underlying manifolds, such as their fundamental and first homology groups. We also contrast early implementations of our techniques with standard software programs for 3-manifolds, achieving better precision and faster algorithms for the average cases and exponential gains in speed for some particular presentations of the inputs.

## 1. INTRODUCTION

Since the early days of computational topology, *3-manifolds* have attracted researchers' keen interest [21, 27, 33] for lying exactly in midway between the well-understood surfaces and the widely behaved 4-manifolds. For example, several 3-manifold problems were related to important questions in complexity theories:  $S^3$  recognition was proved by Schleimer to be in NP [51], whereas approximations of some quantum invariants are firmly tied to quantum computing and are known to be  $\#P$ -hard [1, 2, 16]. The problems of computationally classifying [6, 10, 32] and manipulating the geometry and topology of these spaces [7, 35] have also received significant theoretical and practical attention, with implementations of different algorithms publicly available in the most important software of the field, **regina** [8] and **Snappy** [11]. The greater part of these algorithms assume the 3-manifolds given by triangulations—that is, homeomorphic copies described by a finite set of tetrahedra and gluing rules among their faces—with their run time often measured on the number of tetrahedra. This justifies the usual strategies [5, 8, 11] of simplifying triangulations before computations, but some theoretical bounds [12, 28, 29, 39] can limit the amount of simplification possible, making it necessary to develop algorithms with alternative representations of 3-manifolds in mind.

*Heegaard splittings* are one of these alternatives. They depict a closed 3-manifold  $M$  as the result of gluing two better-behaved pieces called *handlebodies* along a common boundary. Heegaard splittings can also be combinatorially described by *Heegaard diagrams*, two sets of curves in a surface whose intersection pattern conveys a lot of topological information about  $M$ . We suggest here a new data structure to represent Heegaard diagrams based on *normal coordinates*, of a size as large as the *binary* of the number of intersection points between the two sets of curves. The gain in measuring the complexity of 3-manifolds through this notion is not to be overlooked: we present in Remark 5.1 families of manifolds whose complexities of diagrams grow linearly on the size of the input, but whose (direct) triangulations use exponentially many tetrahedra. What is more important, however, is that due to the proliferation of efficient operations on normal coordinates in

---

INRIA d'Université Côte d'Azur, [henrique.lovisi-ennes@inria.fr](mailto:henrique.lovisi-ennes@inria.fr).  
INRIA d'Université Côte d'Azur, [clement.maria@inria.fr](mailto:clement.maria@inria.fr).

the last two decades [18, 34, 48, 49, 55], we are able to establish polynomial time algorithms even in this compressed notion of complexity, leading to basic manipulations of Heegaard splittings and 3-manifolds. We hope that these techniques are useful for the study and classification of topological spaces that are beyond the reach of efficiency when represented by other methods.

This paper starts with a background section on both low-dimensional and computational topology (Section 2), where we review some of the concepts and results that we will need in later sections. To keep this paper short, we refer the reader to [52] and [54] for basic ideas of geometric topology, such as homeomorphisms, isotopies, gluing maps, and manifolds. Our contribution starts in Section 3, where we formally present our data structure for Heegaard splittings. Section 4 establishes some basic algorithms in this structure. We then compare early implementations<sup>1</sup> of these algorithms with triangulation-dependent methods in Section 5. We also present appendices with details on the implementation and extensions of the techniques described in the main text.

Before we close this introduction, we call the reader’s attention to two subtleties of the current work. First, although most of our tools are applicable to *generalized* Heegaard splittings defined for *orientable compact* 3-manifolds, potentially with boundary [31, 52], we will solely focus on *closed* 3-manifolds. Therefore, all 3-manifolds here will be assumed orientable and closed, unless explicitly stated otherwise. Second, we assume throughout a *unit-cost RAM model*, with some bit-size  $W$  [20]. This means that the four integer operations and integer comparisons can be executed in constant time, provided that the numbers involved have binary representations of size at most  $W$ .

#### ACKNOWLEDGEMENT

This work has been partially supported by the ANR project ANR-20-CE48-0007 (AlgoKnot) and the project ANR-15-IDEX-0001 (UCA JEDI). It has also been supported by the French government, through the France 2030 investment plan managed by the Agence Nationale de la Recherche, as part of the “UCA DS4H” project, reference ANR-17-EURE-0004.

## 2. BACKGROUND MATERIAL

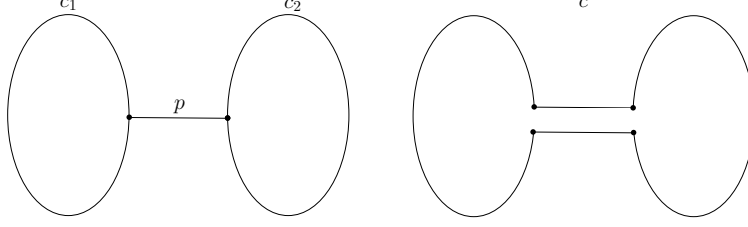
**2.1. Background on low-dimensional topology.** By *surface*, we understand a compact and connected smooth 2-manifold  $\Sigma$  with or without boundary. All surfaces will be assumed orientable and oriented. If  $\Sigma$  is closed, it is uniquely given, up to homeomorphism, by an integer  $g$  called the surface’s genus [19] and we denote this surface by  $\Sigma_g$ . A (*simple closed*) *curve* and an *arc* are images of proper embeddings of  $S^1$  and  $[0, 1]$  in  $\Sigma$ , respectively. A *multicurve* is a finite collection of disjoint curves. Given a multicurve  $\gamma$ , we denote its number of connected components by  $\#\gamma$  and, with some abuse of notation, write  $c \in \gamma$  if  $c$  is a component of  $\gamma$ . Whenever possible, we reserve Greek letters for multicurves and Latin letters for curves and arcs.

We will most often consider the isotopy class of a (multi)curve  $\gamma$  in  $\Sigma$ ,  $[\gamma]$ . A class  $[\gamma]$  is called *essential* if no component is isotopic to point. From now on, we will not differentiate  $\gamma$  from its isotopy class  $[\gamma]$  in the notation if no confusion arises.

Let  $\gamma$  and  $\delta$  be two oriented (multi)curves in  $\Sigma$ , isotoped to intersect transversely. For each intersection point, we let its *index* be  $+1$  if the orientation of the curves agrees with the orientation of  $\Sigma$  as in the right-hand rule, otherwise we set it to  $-1$ . The *algebraic intersection number* of  $\gamma$  and  $\delta$ ,  $\hat{i}(\gamma, \delta)$ , is the sum of the indices of all their transverse intersections; the algebraic intersection number is well defined up to isotopy [19]. Two (multi)curves are said to be in *efficient position* if they are representative of their respective isotopic classes such that the total number of intersection points between them is minimal. Equivalently, they are in efficient position if they do not have segments that cobound disks, known as *bigons*, in the surface [19].

---

<sup>1</sup>The code is publicly available at <https://github.com/HlovisiEnnes/FHDpy>. Details on the implementation are also outlined in Appendix B.

FIGURE 1. The result  $c$  of a band sum of  $c_1$ ,  $c_2$ , and  $p$ .

The *mapping class group* of the surface  $\Sigma_g$ ,  $\text{Mod}(\Sigma_g)$ , is the group of orientation-preserving  $\Sigma_g \rightarrow \Sigma_g$  homeomorphisms up to isotopy. For each  $g$ ,  $\text{Mod}(\Sigma_g)$  is finitely generated as a group by an alphabet  $\mathcal{L}$ , consisting of *Dehn twists* about  $3g - 1$  (isotopy classes of) canonically defined essential curves  $s_1, \dots, s_{3g-1}$  [36]. Formally, a Dehn twist  $\tau_s : \Sigma_g \rightarrow \Sigma_g$  about  $s$  is given by cutting out a cylindrical regular neighborhood around the curve, giving a  $2\pi$  left twist to one of the cylinder's boundaries and gluing the cylinder back into the surface. We call the curves  $s_1, \dots, s_{3g-1}$  the surface's *Lickorish generators*. Hopefully without confusion, we also call the Dehn twists in the alphabet  $\mathcal{L} = \{\tau_{s_1}, \dots, \tau_{s_{3g-1}}\}$  Lickorish generators.

An essential multicurve  $\gamma$  in the surface  $\Sigma_g$  is a *system* if  $\Sigma_g$  cut along  $\gamma$ ,  $\Sigma_g \setminus \gamma$ , is homeomorphic to a  $2g$  punctured sphere. A system  $\gamma$  in  $\Sigma_g$ , for  $g \geq 1$ , can be used to construct the genus  $g$  *handlebody*

$$\mathcal{H}_\gamma = \Sigma_g \times [0, 1] \cup_{\gamma \times \{0\}} 2\text{-handles} \cup 3\text{-handles}$$

where we attach 2-handles along the curves  $\gamma$  in  $\Sigma \times \{0\}$  and fill any spherical boundary component with 3-handles. Note that  $\partial \mathcal{H}_\gamma = \Sigma_g$  and that the handlebody  $\mathcal{H}_\gamma$  is homeomorphic to the connected sum of  $g$  solid tori. The components of  $\gamma$  are *meridians* of  $\mathcal{H}_\gamma$  in the sense that they bound disks in the handlebody's interior. Two systems  $\gamma$  and  $\gamma'$  on the same surface  $\Sigma_g$  will be called *equivalent* if  $\gamma'$  is a set of meridians in  $\mathcal{H}_\gamma$  (which implies that  $\gamma$  is a set of meridians in  $\mathcal{H}_{\gamma'}$ ).

**Remark 2.1.** In this paper, we restrict the analysis to *minimal* systems  $\gamma$ , that is, we assume  $\#\gamma = g$ . In recent decades, it became common to extend systems to any multicurve in the surface that defines a handlebody [25, 56]. In fact, the data structure described in Section 3 can be generalized to this notion of system and there are algorithms to translate from and to the special case of cardinality  $g$ . For completeness, we describe these extensions in the Appendix A.

Let  $c_1, c_2$  be two fixed components of a system  $\gamma$  and  $p$  an arc from a puncture corresponding to  $c_1$  to a puncture corresponding to  $c_2$  in  $\Sigma_g \setminus \gamma$ . We define the *band sum* of  $c_1, c_2$  and  $p$  as the curve  $c$  in  $\Sigma_g \setminus \gamma$  indicated by the surgery in Figure 1. One can show that  $c$  is essential and bounds a disk in  $\mathcal{H}_\gamma$  [16, 31], implying that  $\gamma' = \gamma - \{c_1\} \cup \{c\}$  is a system equivalent to  $\gamma$ . We call this whole operation a *disk slide*. With finitely many applications of disk slides and isotopies, a system  $\beta$  can be transformed into any equivalent system  $\beta'$  [31].

A genus  $g$  *Heegaard splitting* is the closed 3-manifold resulting from a gluing of two handlebodies with boundaries homeomorphic to  $\Sigma_g$  through a gluing map  $f : \Sigma_g \rightarrow \Sigma_g$ . In fact, one might assume that  $f$  is given by a  $\phi \in \text{Mod}(\Sigma_g)$  composed with some canonical orientation-reversing homeomorphism. This means that a Heegaard splitting can be given by a pair  $(\Sigma_g, \phi)$  where  $\phi$  is a word on Lickorish generators. We call this presentation of Heegaard splittings a *Heegaard word*. Every closed 3-manifold has a Heegaard splitting and can then be associated with some pair  $(\Sigma_g, \phi)$  [43, 47].

Although naturally combinatorial, a Heegaard word  $(\Sigma_g, \phi)$  hardly conveys topological information about the closed 3-manifold  $M$  that it represents. Nonetheless, if we fix a system of meridians  $\alpha$  on one of the two handlebodies,  $\mathcal{H}_\alpha$ , then  $\beta = \phi(\alpha)$  is a system of meridians of the *other* handlebody,  $\mathcal{H}_\beta$ . We call the tuple  $(\Sigma_g, \alpha, \beta)$  a *Heegaard diagram*. We note that Heegaard diagrams

are algorithmically independent from Heegaard words: any two systems  $\alpha$  and  $\beta$  will define the same splitting, provided that the curves are meridians in their respective handlebodies. Diagrams are therefore not unique for a given splitting. For example, if  $\beta$  and  $\beta'$  are *isotopic diagrams* on  $\Sigma_g$ —that is,  $\beta$  and  $\beta'$  are isotopic multicurves in  $\Sigma_g$ —then  $(\Sigma_g, \alpha, \beta)$  and  $(\Sigma_g, \alpha, \beta')$  naturally define the same manifold. Similarly, if  $\beta$  is equivalent to  $\beta'$ , we say that the diagrams are *equivalent* and note that  $(\Sigma_g, \alpha, \beta)$  and  $(\Sigma_g, \alpha, \beta')$  also define the same 3-manifold.

*Stabilizations* provide of yet another method to generate alternative Heegaard splittings of a same 3-manifold. Formally, let  $(\Sigma_{g_1}, \alpha_1, \beta_1)$  be a Heegaard diagram of a 3-manifold  $M_1$  and  $(\Sigma_{g_2}, \alpha_2, \beta_2)$  a diagram of  $M_2$ . The diagram  $(\Sigma_{g_1+g_2}, \alpha_1 \cup \alpha_2, \beta_1 \cup \beta_2)$  represents the connected sum  $M_1 \# M_2$ , where  $\Sigma_{g_1+g_2}$  is the connected sum of  $\Sigma_{g_1}$  and  $\Sigma_{g_2}$  taken along open disks disjoint from  $\alpha_1, \alpha_2, \beta_1$ , and  $\beta_2$ . In particular, noting that  $S^3$  has a splitting with diagram  $(\Sigma_1 = T^2, m, \ell)$ , where  $|m \cap \ell| = 1$ , and that  $M \# S^3$  is homomorphic to  $M$ , the splitting  $(\Sigma_{g+1}, \beta \cup \{\ell\})$  represents the same manifold as  $(\Sigma_g, \alpha, \beta)$ . We say that the former is a *stabilization* of the latter. In the other direction, a Heegaard diagram  $(\Sigma_g, \alpha, \beta)$  represents a stabilization of a lower genus splitting if and only if there is a meridian  $a$  in  $\mathcal{H}_\alpha$  and a meridian  $b$  in  $\mathcal{H}_\beta$  such that  $|a \cap b| = 1$  [31]. In particular, we say that this pair of meridians is a *stabilization pair* and that the diagram is *stabilized*. For a Heegaard diagram  $(\Sigma_g, \alpha, \beta)$ , we say that  $a$  and  $b$  form a *trivial stabilization pair* if  $a$  is a component  $\alpha$ ,  $b$  is a component of  $\beta$ , they form a stabilization pair, and  $b \cap a' = \emptyset$  and  $b' \cap a = \emptyset$  for any other component  $a' \in \alpha$  and  $b' \in \beta$ . Whenever  $a$  and  $b$  form a trivial stabilization, cutting the surface along  $a$  induces a Heegaard diagram in the surface of genus one unit smaller. This process will be called *destabilization*.

A splitting  $(\Sigma_g, \mathcal{H}_\alpha, \mathcal{H}_\beta)$  is called *reducible* if there is a curve  $c$  in  $\Sigma_g$  that is a meridian of both  $\mathcal{H}_\alpha$  and  $\mathcal{H}_\beta$ . We call a diagram  $(\Sigma_g, \alpha, \beta)$  *reducible* if either (1) there are a component  $a \in \alpha$  and a component  $b \in \beta$  that are isotopic in  $\Sigma_g$ ; or (2) if there is an essential separating curve  $s$ , disjoint from both  $\alpha$  and  $\beta$ , and such that  $\Sigma_g \setminus s$  defines a connected sum of two Heegaard splittings. The uniqueness of fundamental group decomposition [3] and [52][Theorem 6.3.5] imply that a reducible diagram represents a reducible splitting. A 3-manifold is *reducible* if it contains a sphere that does not bound a ball. If  $(\Sigma_g, \alpha, \beta)$  is stabilized, then either the splitting is reducible or a stabilization of a genus 1 splitting of  $S^3$ ; moreover, a reducible splitting is stabilized or the splitting of a reducible manifold [31].

Useful algebraic information on the 3-manifold can also be readily obtained from its Heegaard diagrams. Label the curves  $a_1, \dots, a_g \in \alpha$  and  $b_1, \dots, b_g \in \beta$  and give each of them an orientation. It follows from an application of the Van Kampen theorem [22, 26, 31] that we can compute a presentation  $\langle x_1, \dots, x_g | r_1, \dots, r_g \rangle$  for the *fundamental group*  $\pi_1(M)$  by traversing the curve  $b_i$  along the assumed orientation and, whenever it intersects some  $a_j$ , we append  $x_j$  to the relation  $r_i$  if the index of the intersection is positive, otherwise we append  $x_j^{-1}$  to it (if  $b_i$  does not intersect  $\alpha$ ,  $r_i$  is just the trivial relation).

Now, recall that the *first (integral) homology group* of  $M$ ,  $H_1(M)$ , is isomorphic to the abelianization of  $\pi_1(M)$  [22]. We may therefore present  $H_1(M)$  as

$$\langle x_1, \dots, x_g | r'_1, \dots, r'_g, [x_i, x_j], 1 \leq i < j \leq g \rangle,$$

where each  $r'_i = x_1^{k_i^1} \dots x_g^{k_i^g}$  can be computed by commuting the generators  $x_j$  in the relations  $r_i$ . Note that  $k_i^j = \hat{i}(b_i, a_j)$  and we store this information in a  $g \times g$  *presentation matrix* for  $H_1(M)$ ,  $K = [k_i^j]$ , whose Smith normal form carries all the necessary information about this Abelian group. For example, the *(first) Betti number* of  $M$  is given by the number of zero-rows. A 3-manifold with Betti number equal to zero is called a *rational homology sphere*, and it will be an *integral homology sphere* if the Smith form of the presentation matrix is the identity.

**2.2. Background on computational topology.** Heegaard diagrams consist of three essential components that any candidate data structure must encode: a surface,  $\Sigma_g$ , and two multicurves,

$\alpha$  and  $\beta$ . Starting with the surface, a graph  $T = (V, E)$  embedded in  $\Sigma$  is a *cellular embedding* if the manifold defined by cutting  $\Sigma$  along  $T$ ,  $\Sigma \setminus T$ , is homeomorphic to a collection of disks. We call each disk component of  $\Sigma \setminus T$  a *face* of  $T$ . A cellular embedding  $T$  in the surface  $\Sigma$  is said to be *oriented* if we assign to each face an ordered list of its vertices, consistent with the orientation of  $\Sigma$  as in the right-hand rule. We assume every cellular graph to be oriented. A cellular embedding  $T$  is a (*generalized*) *triangulation* of  $\Sigma$  if exactly three edges of  $T$  bound (the closure of) each face. We define the size of a triangulation,  $|T|$ , as its number of faces; note that  $|T| = O(|E|)$  where  $|E|$  is the number of edges of the triangulation. Surface triangulations are not to be confused with the similar, but different concept of 3-manifold triangulations.

Every oriented surface can be described as a data structure by an oriented triangulation. For the triangulations themselves, we will assume that they are given by the set of vertices, edges, and triangles, with bidirectional pointers between vertices and edges and between edges and the triangles. In particular, determining whether two triangles are adjacent, getting the incident vertices and edges of a triangle, and finding triangles bounded by a specific edge take constant time in this model. Other more compact data structures for triangulation, such as CGAL's [13], can be converted into our structure in time  $O(|T|)$  and at similar costs to memory. More general cellular embeddings are treated similarly.

A curve  $c$  is *edged* with respect to  $T$  if it is disjoint from its faces. We represent an edged curve as a data structure by the list  $E_T(c) = \{e \in E : |c \cap e| = e\}$ , assumed ordered according to an implicit traversing orientation of  $c$ . Similarly, a multicurve  $\gamma$  can be represented by a set of  $\#\gamma$  edge lists, one for each component, which we denote as  $E_T(\gamma)$ . Although we assume that no two components of  $\gamma$  share an edge, they might share vertices. The *complexity* of  $E_T(\gamma)$  is  $\|E_T(\gamma)\| = \sum_{c \in \gamma} |E_T(c)|$ .

On the other hand, an essential multicurve  $\gamma$  is called *standard* in  $T$  if it intersects the graph only at the edges and transversely. If  $\gamma$  is standard, we can represent it as a collection of words in a finite alphabet: we arbitrarily orient the edges  $E$  and take  $E^\pm = E \cup E^{-1}$  for the letters. Then for each component  $c$  of  $\gamma$ , the word  $I_T(c)$  in  $(E^\pm)^*$  is given by traversing  $c$  along some arbitrary direction and, whenever we intersect an edge  $e \in E$ , we append  $e^i$  to  $I_T(c)$  where  $i$  is the index of the intersection. An *intersection sequence* representation for  $\gamma$ ,  $I_T(\gamma)$ , is the set  $\{I_T(c)\}_{c \in \gamma}$ . Note that while the  $E_T(\gamma)$  is well-defined at the multicurve level, intersection sequences are defined only up to isotopies inside the cellular graph's faces. Moreover, cyclic permutations and taking inverses of the words  $I_T(c)$  in  $I_T(\gamma)$  define the same isotopy class.

Instead of working with explicit intersection sequences, we will often assume *straight line programs* (SLPs) to express  $I_T(c)$ . Formally, an SLP on the alphabet  $E^\pm$  is a finite sequence of equations  $\langle x_1 = \text{EXPR}_1, \dots, x_\ell = \text{EXPR}_\ell \rangle$ , where the left-hand side,  $x_i$ , are symbols not in  $E^\pm$  called *variables* and the expressions on the right-hand side,  $\text{EXPR}_i \in (E^\pm \cup \{x_1, \dots, x_{i-1}\})^*$ , are called *assignments*. Each assignment  $\text{EXPR}_i$  is assumed to be either a symbol from  $E^\pm$ , in which case the assignment is called *simple*, or of form  $\text{EXPR}_i = x_{j_1}^{\pm 1} \cdot x_{j_2}^{\pm 1} \cdots x_{j_k}^{\pm 1}$ , where  $1 \leq j_1, \dots, j_k < i$ , in which case we say that the assignment is *proper*. In particular, the SLP  $\langle x_1, \dots, x_\ell \rangle$  represents a word  $w$  in  $(E^\pm)^*$  if, by recursively substituting the appropriate  $x_j$  in each proper assignment, gives  $x_\ell$  equal to  $w$ . We call  $\ell$  the *length* of the SLP and define its *complexity*  $m = \sum_{i=1}^\ell |\text{EXPR}_i|$ , where  $|\text{EXPR}_i|$  is the number of variables and symbols in the assignment  $|\text{EXPR}_i|$ . Given any word  $e_1 \dots e_n$  in  $(E^\pm)^*$ , one can trivially build an SLP of complexity  $2n$ , but there are instances in which SLPs can be used to give exponential gains over uncompressed representation of words [49]. Nonetheless, even in these extremely compressed cases, several useful operations can still be efficiently performed in the SLP's complexity, as stated in the following lemma. Here and throughout, we assume that  $\lg k$  is the number of bits necessary to represent the potentially signed integer  $k$ ; in particular,  $\lg k = \log k + 2$  if  $k$  is signed and  $\log k + 1$  if unsigned.

**Lemma 2.2.** *Let  $\langle x_1, \dots, x_\ell \rangle$  be an SLP of complexity  $m$  representing a word  $w \in (E^\pm)^*$ . In a unit-cost RAM model of bit-size  $m + \lg k$ , for a fixed  $k \in \mathbb{Z}^+$ , one can compute*

- (a) an SLP of  $w^{-1}$  in time  $O(1)$ ;
- (b) an SLP of  $w^k$  in time  $O(\lg k)$ ;
- (c) the number of occurrences of a symbol  $e \in E^\pm$  in  $w$ ,  $e(w)$ , in time  $O(m)$ .

*Proof.* For (a), note that  $\langle x_1, \dots, x_\ell, x_\ell^{-1} \rangle$  is an SLP for  $w^{-1}$ . For (b), assume  $k \geq 0$  (the case for  $k < 0$  follows from this and (a)) and let  $b_0 b_1 \dots b_{\lg k}$  be the binary expansion of  $k$ , then

$$\langle x_1, \dots, x_\ell, x_{\ell+1} = x_\ell \cdot x_\ell, \dots, x_{\ell+\lg k} = x_{\ell+\lg k-1} \cdot x_{\ell+\lg k-1}, b_0 x_\ell \cdot b_1 x_{\ell+1} \cdot \dots \cdot b_{\lg k} x_{\ell+\lg k} \rangle$$

is an SLP for  $w^k$ . Finally, (c) follows by dynamic programming through iterating over  $1 \leq i \leq \ell$  and counting the references to the simple assignment  $x_j = e$  or to proper assignments that recursively refer to assignments that refer to  $x_j$ .  $\square$

We will assume that every intersection sequence  $I_T(c)$  is given by an SLP of complexity  $\|I_T(c)\|$  and let  $\|I_T(\gamma)\| = \sum_{c \in \gamma} \|I_T(c)\|$ .

Now, suppose that  $T = (V, E)$  is a triangulation. A standard (multi)curve  $\gamma$  is *normal* if its intersection with each face of  $T$  are arcs, called *elementary arcs*, that connect distinct sides of the triangle in which they are contained. Equivalently,  $\gamma$  is normal if each (uncompressed) intersection sequence in  $I_T(\gamma)$  is *cyclic reduced*, that is, if there are no substrings of type  $ee^{-1}$  or  $e^{-1}e$  in any of the cyclic permutation of the components' sequences. When the curve  $c$  is normal for a triangulation, its isotopy class is fixed by the number of times it intersects each labeled edge [48], implying that we can describe it through a vector in  $N_T(c)$  in  $\mathbb{N}^{|E|}$ . We call  $N_T(c)$  the curves' *normal coordinates*, whose complexity,  $\|N_T(c)\|$ , is the number of bits necessary to store this vector, i.e.,  $\sum_{e \in E} \lg e(c) = \sum_{e \in E} (\log e(c) + 1)$ . Naturally, we define  $N_T(\gamma)$  as the set  $\{N_T(c)\}_{c \in \gamma}$ .

**Remark 2.3.** We could equally represent a normal multicurve  $\gamma$  with a *single* vector  $\sum_{c \in \gamma} N_T(c)$ . Similarly, it is possible and common to extend the notion of SLPs to encode more than one uncompressed word, which in our case, implies giving all components of  $\gamma$  as a single SLP. Although these approaches are more parsimonious, they are less useful for our needs. Moreover, Lemma 5.1 of [18] gives an algorithm to transform, in time  $O(|T| \|N_T(\gamma)\|)$ , the normal coordinates of a multicurve given by a sum of its components' coordinates to our expected form.

Any normal (multi)curve  $\gamma$  partitions the edges of  $T$  into segments called *ports*. The *overlay graph* of  $\gamma$  is defined by having as vertices the union of  $V$  and the intersections  $E \cap \gamma$ , and as edges the union of the ports and the elementary arcs of  $\gamma$  (see Figure 2). The overlay graph splits each triangle  $t$  of the original triangulation into two types of regions: *junctions*, which are adjacent to tree edges of  $T$ , and *blocks*, which are adjacent to only two. A port of the overlay graph is called *redundant* if it separates blocks from different triangles of the original triangulation. Following Erickson and Nayyeri, we define the *street complex* of  $\gamma$ ,  $S(T, \gamma)$ , by deleting redundant ports and their endpoints from the overlay graph. In practice, the street complex merges blocks of the overlay graph into longer faces called *streets*; naturally,  $S(T, \gamma)$  is a cellular graph in the surface triangulated by  $T$ , see Figure 2. We define the *crossing sequence* of a street in  $S(T, \gamma)$  as the intersection sequence of a curve that crosses the street from one end to the other with respect to the original triangulation  $T$ . For simplicity, we assume that any port that separates two junctions is a degenerate street with a crossing sequence of length 1. The street complexes of all multicurves in this paper will have complexity  $O(|T|)$  [18].

### 3. DATA STRUCTURE FOR HEEGAARD DIAGRAMS

Normal coordinates suggest a very natural encoding of Heegaard diagrams and, consequently, of closed 3-manifolds. Explicitly, we propose representing a diagram  $(\Sigma_g, \alpha, \beta)$  by a tuple  $(T, E_T(\alpha), N_T(\beta))$ , where  $T = (V, E)$  is a triangulation,  $E_T(\alpha)$  is an edge representation of  $\alpha$ , and  $N_T(\beta)$  is a normal

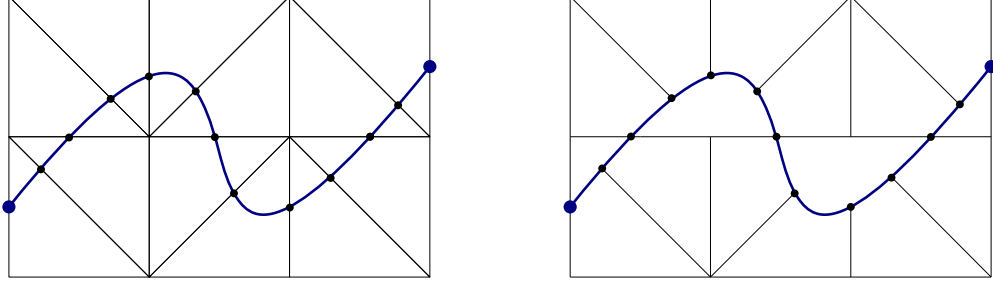


FIGURE 2. Left: the overlay graph of a normal arc (blue) with respect to a triangulation (black). Right: its street complex.

coordinate representation of  $\beta$ . We will often refer to the pair  $(T, E_T(\alpha))$  as a *marked triangulation* of  $\Sigma_g$ , in which context  $N_T(\beta)$  will be called the diagram itself. The *complexity* of the diagram is

$$(3.1) \quad \|(T, E_T(\alpha), N_T(\beta))\| = |T| + \|E_T(\alpha)\| + \|N_T(\beta)\|.$$

We note that  $\|E_T(\alpha)\| = O(|T|) = O(\|N_T(\beta)\|/|\beta \cap E|)$ , that is, for complexity purposes, only the last term of (3.1) matters. Nonetheless, for the sake of clarity, we will still refer to the terms of equation (3.1) arising from the marked triangulation in our analyses. All complexities will be reported under the assumption that  $|\beta \cap T| = \Omega(|T|^2)$  as, otherwise, there exist some faster trivial algorithms.

**Remark 3.2.** For implementation purposes, especially in the context of Section 5, it is convenient to use the polygon representations of closed surfaces [22] to recursively define a sequence of marked triangulations  $T_g$  of  $\Sigma_g$ , with  $|T_g| = \Theta(g)$  and all Lickorish generators edged in  $T_g$ .

Our choices of data structures for  $\alpha$  and  $\beta$  allow us to represent curves with exponentially many intersection points with respect to the complexity of the diagram. Referring to the discussion at the end of Section 2.1, more intersections may lead to more complicated fundamental groups and, consequently [39][Proposition 2.6.6], more complicated 3-manifolds. In this sense, our structure is significantly more compressed than representations of Heegaard diagrams with *both*  $\alpha$  and  $\beta$  edged, which can have, at most,  $E_T(\alpha) \times E_T(\beta) = O(|T|^2)$  many intersection points. This means that, while there exist efficient algorithms to transform from the fully edged representation of Heegaard diagrams to ours—see Lemma 3.5—the other direction is considerably harder.

Complexity gains are also noticeable when we compare our structure with triangulations of 3-manifolds. For example, while there exist algorithms to triangulate Heegaard diagrams [24], they take polynomial time on the number of intersection points between  $\alpha$  and  $\beta$ . Moreover, as we empirically verify in Section 5, converting a Heegaard word to a diagram can be exponentially faster than converting the word to a triangulation for some particular inputs and, at least as fast, for the general case. On the downside, it is unclear how to obtain and manipulate geometric information (such as *hyperbolicity*) or to compute certain quantum invariants directly from Heegaard diagrams, making triangulations still preferable for these kinds of problem.

As stated in the introduction, our goal is to establish basic efficient algorithms even in this very compressed setting. For such a purpose, we will make extensive use of the next two results. The first of them is (almost) fully established by Erickson and Nayyeri [17].

**Theorem 3.3.** *Suppose that  $(T, E_T(\alpha), N_T(\beta))$  is a genus  $g$  Heegaard diagram of complexity  $m$ . In a unit-cost RAM model of bit-size  $\log |\beta \cap E| = O(m/|T|)$ , one may compute*

- (a) *the street complex  $S(T, \beta)$  in time  $O(m|T|)$ ;*
- (b) *SLPs of the crossing sequence of all streets of  $S(T, \gamma)$  in time  $O(m|T|)$  of total complexity  $O(m|T|)$ ;*

(c) the SLPs  $I_T(\beta)$  of complexity  $O(m)$ , in time  $O(m)$ .

*Proof.* Part (a) corresponds to Theorems 4.7 of [18]. Part (b) follows from Theorem 4.8 of the same paper, where we simply add the variable corresponding to the desired street at the end of the SLP compressing the crossing sequences of all components of  $\beta$ . For part (c), use Lemma 3.4.2 in [55].  $\square$

**Remark 3.4.** A conceptually simpler algorithm for part (c) of Theorem 3.3 using only the methods of [18] is possible, but it outputs SLPs of complexity  $O(m|T|)$ .

For the next theorem, we might assume that a Heegaard word  $\phi$  is given in *power-notation form*, that is,  $\phi = \tau_{s_n}^{k_n} \circ \dots \circ \tau_{s_1}^{k_1}$ ,  $s_i \neq s_{i+1}$  for  $1 \leq i < n$ , and with each  $k_i \in \mathbb{Z}$  in signed binary. A *fully uncompressed* Heegaard word  $\phi' = \tau_{s'_1}^{\pm 1} \circ \dots \circ \tau_{s'_{|\phi'|}}^{\pm 1}$ , with some  $s'_i$  potentially equal to  $s'_{i+1}$ , can be put in power-notation in time  $O(|\phi'|)$  with a unit-cost RAM model of bit-size  $\lg |\phi'|$ . For convenience, we shall also assume that the Lickorish generators are given as edge curves with respect to  $T$ . Nonetheless, even if we suppose that  $\mathcal{L}$  is given through normal coordinates or intersection sequences, the theorem still holds with similar complexity bounds by multiple applications of Theorem 4.9. Before we go to the main result, we state the following lemma.

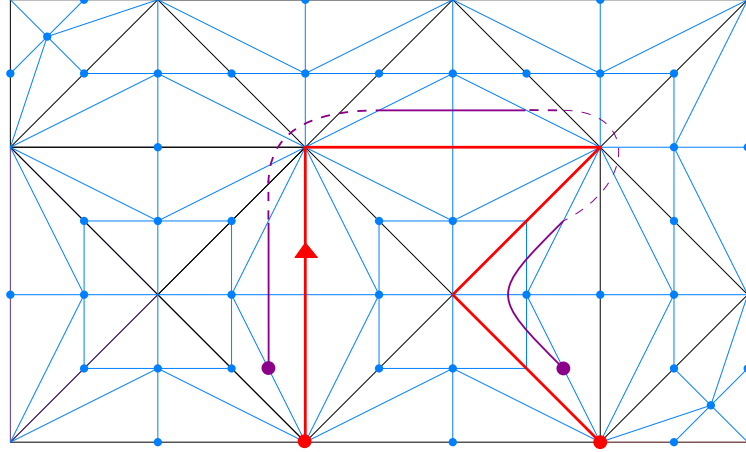
**Lemma 3.5.** *Let  $E_T(\gamma)$  be an edge list representation of an essential multicurve  $\gamma$  in the surface  $\Sigma_g$ , with triangulation  $T$ . One can compute, in time  $O(\#\gamma \times |T|)$ , a set of SLPs of complexity at most  $O(\#\gamma \times |T|)$  of the intersection sequences of a normal multicurve  $\gamma'$ , isotopic to  $\gamma$  in  $\Sigma_g$ .*

*Proof of 3.5.* Suppose  $\gamma$  is a simple curve. We can obtain, in time  $O(|T|)$ , the first barycentric subdivision  $T'$  of the triangulation  $T$  [22], which we note to have size  $|T'| = 6|T|$  (see blue edges and vertices of Figure 3a). We resort to  $T'$  to guarantee that no two vertices or edges of a same triangle are identified. One can easily update the representation  $E_T(\gamma)$  to  $E_{T'}(\gamma)$  in time  $O(|T|)$ . Because  $T'$  is assumed oriented, for each edge  $e_i \in E_{T'}(\gamma)$ , we can get, in time  $O(1)$  on our data structure, the triangle  $t_i$  to the left of  $e_\gamma$  according to the traversing direction of  $\gamma$  as defined by  $E_{T'}(\gamma)$ . With the information of  $t_i$ , we can query on the other two edges  $f_{i,1}, f_{i,2}$  of  $t_i$  distinct from  $e_i$  and on the indices of the intersections,  $k_{i,1}, k_{i,2} = \pm 1$  of a directed arc in  $t_i$  parallel to  $e_i$ . We also denote by  $v_i$  the unique vertex of  $t_i$  incident to  $e_i$  and  $e_{i+1}$  (uniqueness is guaranteed by the barycentric subdivision). We will iterate over the tuples  $(f_{i,1}^{k_{i,1}}, f_{i,2}^{k_{i,2}}, v_i, t_i)$ ,  $1 \leq i \leq \|E_T(\gamma)\|$ , to construct an uncompressed intersection sequence,  $w_\gamma$ , of a standard curve  $\gamma'$  (purple in Figure 3a) isotopic to  $\gamma$ .

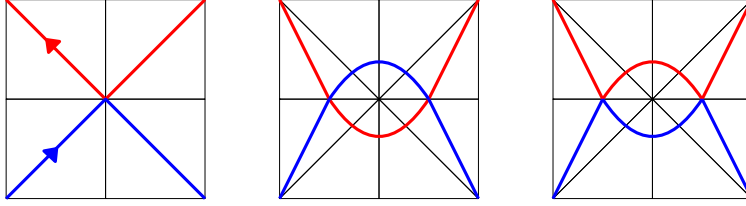
Attach  $f_{i,1}^{k_{i,1}}$  to  $w_\gamma$ . Call  $(t')_i^1$  the triangle adjacent to  $t_i$  by the edge  $f_{i,2}$ ; note that  $(t')_i^1$  is also incident to  $v_i$ . Again, because of the barycentric subdivision, there is exactly one edge  $(f')_{i,2}^1$  distinct from  $(f')_{i,1}^1 = f_{i,2}$  incident to  $v_i$ . The pair  $((f')_{i,1}^1, (f')_{i,2}^1)$  defines an elementary arc in  $(t')_i^1$  given by an intersection sequence  $((f')_{i,1}^1, (f')_{i,2}^1)$  (we here hide the indices of intersection to simplify the notation), see the dashed purple lines in Figure 3a. Similarly and recursively, the triangle  $(t')_i^2$  that shares  $(f')_{i,2}^1$  with  $(t')_i^1$  has exactly one other edge, call it  $(f')_{i,2}^2$ , incident to  $v_i$ . Because  $f_{i,1}^{k_{i,1}}$  is incident to  $v_i$ , we can repeat the process until  $(f')_{i+1,2}^n = f_{i,1}^{k_{i,1}}$  for some  $n \leq 3|T'|$ . We then append  $(f')_{i,1}^1, (f')_{i,1}^2, \dots, (f')_{i,1}^n, f_{i+1,1}$  to  $w_\gamma$ . Since the curve  $\gamma$  is assumed simple, no edge or vertex occurs twice in the list  $E_T(\gamma)$ , meaning that this process takes time, at most,  $O(|T'|) = O(|T|)$ . We then remove edges in  $T' - T$  from  $w_\gamma$  and cyclically reduce it to guarantee that it represents a normal curve. Finally,  $w_\gamma$  can be transformed into a trivial SLP,  $I_T(\gamma)$ , in time  $O(|w_\gamma|) = O(|T|)$ .

Now, assume that  $\#\gamma \geq 2$  and suppose we separately apply the above procedure to each component  $c_1, \dots, c_{\#\gamma}$  of  $\gamma$ , obtaining uncompressed sequences  $w_1, \dots, w_{\#\gamma}$ . Although these sequences individually represent curves that are isotopic to the components of  $\gamma$ , tracing them might cause some intersection between two components, say  $c_1$  and  $c_2$ , if  $E_T(c_1)$  and  $E_T(c_2)$  shared a vertex, as





(A) The triangulation  $T$  (black) and the new edges and vertices introduced by its barycentric subdivision (blue). In red, we show a section of the edged curve  $\gamma$  and the orientation induced by  $E_T(\gamma)$ . In purple, we highlight the standard curve  $\gamma'$  isotopic to  $\gamma$ , where the solid intervals are those obtained by displacing the edges of  $E_T(\gamma)$  and the dashed are those of form  $(f')_{i,1}^j, (f')_{i,2}^j$ .



(B) Left: The possible intersection of the components  $c_1$  and  $c_2$ . Middle: the tracing induced by  $w_1$  and  $w_2$  before the removal of bigons. Right: the surgery to remove bigons between  $c_1$  and  $c_2$ .

FIGURE 3

shown in Figure 3b. One can detect these cases in time  $O(\#\gamma \times \|E_T(\gamma)\|)$  and solve the intersections by exchanging the parts of the sequence  $w_1$  with the parts of the sequence  $w_2$  that cobound bigons, ultimately performing the surgery in the bottom of Figure 3b. We then cyclically reduce each curve  $w_1, \dots, w_{\#\gamma}$ —note that the cyclic reductions cannot form new bigons between components—and compute the trivial SLPs.  $\square$

**Theorem 3.6.** *Suppose  $\phi = \tau_{s_n}^{k_n} \circ \dots \circ \tau_{s_1}^{k_1}$ ,  $s_i \neq s_{i+1}$  for  $1 \leq i < n$ , is a Heegaard word in  $\text{Mod}(\Sigma_g)$  and let  $T$  be a triangulation of  $\Sigma_g$  with  $\alpha$  and Lickorish generators edged. There is an algorithm to compute intersection sequences  $I_T(\phi(\alpha))$  in time  $\Theta(g|T| + n|T|\lg k)$  in a unit-cost RAM model of bit-size  $\lg k$  where  $\lg k = \sum_{i=1}^n \lg k_i$ . Moreover, the Heegaard diagram  $(T, E_T(\alpha), N_T(\phi(\alpha)))$  of complexity  $O(|T|^3 \lg^2 k)$  can be computed in time  $O((|T|\lg k)^{10})$ .*

*Proof.* For each  $s \in \mathcal{L}$ , denote its edge list by  $E_T(s) = \{e_{s,1}, \dots, e_{s,\|E_T(s)\|}\}$ , where  $e_{s,j} \in E$  for  $1 \leq j \leq \|E_T(s)\|$ , and define  $I_T(s, j)$  as (an SLP of) the intersection sequence of a normal curve isotopic to  $s$  starting at a face adjacent to  $e_{s,j}$ . We can use Lemma 3.5 to compute  $I_T(s, j)$  for each  $1 \leq j \leq \|E_T(s)\|$  in time  $O(g|T|)$ . We also compute  $I_T(a)$  for each  $a \in \alpha$ ; in total, this initial step takes time  $O(g|T|)$ .

Let  $I_T(\beta_0) = I_T(\alpha)$ . Assuming  $k_i > 0$ , we recursively construct  $I_T(\beta_i)$ , for  $1 \leq i \leq n$ , by replacing any occurrence of an edge  $e_{s_i,j} \in E_T(s_i)$  in the SLPs  $I_T(\beta_{i-1}) = \{x_1 = \text{EXPR}_1, \dots, x_p = \text{EXPR}_p\}_{b \in \beta}$  with an SLP  $\langle y_1, \dots, y_q \rangle$  of  $I_T(s_i)^{k_i} \cdot s_{i,j}$ , that is,

$$I_T(\beta_i) = \{y_1, \dots, y_q, x'_{q+1} = \text{EXPR}'_1, \dots, x'_{q+p} = \text{EXPR}'_q\}_{b \in \beta}$$

where  $\text{EXPR}'_r$  is the word  $\text{EXPR}_r$  with each occurrence of  $x_t$  substituted by  $x'_{p+t}$  and each occurrence of  $s_{i,j}$  substituted by  $y_q$ . The case of  $k_i < 0$  is treated similarly. By Lemma 2.2, we note that this can be done in time  $O(\|I_T(\beta_{i-1})\| + \lg k_i \|I_T(s_i)\|)$  in the assumed model of computation. In particular,  $I_T(\beta_i)$  is an intersection sequence representation of  $\beta_i = \tau_{s_i}^{k_i} \circ \dots \circ \tau_{s_1}^{k_1}(\alpha)$  and has complexity

$$\begin{aligned} O(\|I_T(\beta_i)\|) &= O(\|I_T(\beta_{i-1})\| + \lg k_i \|I_T(s_i)\|) \\ &= O\left(\|I_T(\alpha)\| + \sum_{i'=1}^i \lg k_{i'} \|I_T(s_{i'})\|\right) \\ &\leq O\left(|T| + |T| \sum_{i'=1}^i \lg k_{i'}\right) = O\left(|T| \sum_{i'=1}^i \lg k_{i'}\right), \end{aligned}$$

where in the second line we recursively applied the equation of the first. The total time to compute  $I_T(\beta) = I_T(\beta_n)$  is bounded by  $n \times \|I_T(\beta)\| = O(n|T| \lg k)$ , and, in the case  $k_i = 1$  for all  $1 \leq i \leq n$ , this becomes  $\Theta(n^2|T|) = \Theta(n|T| \lg k)$ .

For the second part, note that while  $I_T(\beta)$  is, by construction, standard in  $T$ , it might not be normal. We can use the main algorithm of [42] to deterministically compute, in time  $O(\|I_T(\beta)\|^{10})$ , cyclic reduced SLPs for  $\beta$  with complexity  $O(\|I_T(\beta)\|^2)$ . Alternatively, this can be done using a randomized algorithm in time  $O(\|I_T(\beta)\|^3)$  with some probability of error at most  $\delta$  and in a unit-cost RAM model of bit-size  $O(\|I_T(\beta)\| + \lceil 1/\delta \rceil)$ . Part (c) of Lemma 2.2 finishes the proof.  $\square$

#### 4. ALGORITHMS ON HEEGAARD DIAGRAMS

We here describe some polynomial time algorithms and operations on a genus  $g$  Heegaard diagram  $(T, E_T(\alpha), N_T(\beta))$  with complexity  $m$  and representing a closed 3-manifold  $M$ . For convenience, the algorithms and their complexity are summarized in Table 1. For the reported complexities, we assume a unit-cost RAM model of bit-size  $\log |\beta \cap E| = O(\|N_T(\beta)\|/|T|)$ .

**Theorem 4.1 (CHECK DIAGRAM).** *There is an algorithm to check, in time  $O(m|T|)$ , whether a normal multicurve  $\beta$  of complexity  $m$  defines a Heegaard diagram.*

*Proof.* Use a generalization of Theorem 3.3 [17][Theorem 6.5] to trace the street complex  $S(T, \beta)$ , this naturally induces triangulations of the components in  $T \setminus \beta$ , which, following [18], we call *pieces*. We compute the Euler characteristic of each piece in time  $O(|T|)$  [17], ultimately giving their genus. The vectors  $N_T(\beta)$  define a Heegaard splitting if and only if the only piece is a  $2g$ -punctured sphere.  $\square$

**Theorem 4.2 (GET EFFICIENT POSITION).** *There is an algorithm to isotope  $\alpha$  and  $\beta$  to efficient position in  $\Sigma_g$  in time  $O(\text{poly}(m, |T|))$ .*

*Proof.* An algorithm for this problem is described by Lackenby in Theorem 6.3 of [34], where we implicitly use the content of his Corollary 6.5, that is, the number of bigons between the  $\alpha$  and  $\beta$  curves is upper bounded by  $154|T|$ .  $\square$

**Theorem 4.3 (CHECK ISOTOPY).** *There is an algorithm to check, in time  $O(\text{poly}(m, |T|))$ , whether two Heegaard diagrams,  $\beta$  and  $\beta'$  of complexity at most  $m$  are isotopic.*

*Proof.* Once more, this follows from Lackenby's paper [34], this time, from Theorem 1.2.  $\square$

Algorithm name	Description	Complexity	Reference
CHECK DIAGRAM	Decide if normal coordinates define a diagram	$O(m T )$	Theorem 4.1
GET EFFICIENT POSITION	Put $\alpha$ and $\beta$ curves in efficient position	$O(\text{poly}(m,  T ))$	Theorem 4.2
CHECK ISOTOPY	Decide if two diagrams of complexity $m$ , on the same marked triangulation, are isotopic	$O(\text{poly}(m,  T ))$	Theorem 4.3
DO A PACHNER MOVE	Do a Pachner move in the underlying triangulation	$O(1)$	Theorem 4.4
DO A DISK SLIDE	Slide a disk $b_i$ over a disk $b_j$	$O(m T )$	Theorem 4.5
DO STABILIZATION	Compute a stabilization of the diagram	$O(1)$	Theorem 4.6
DO DESTABILIZATION	Detect if there is a trivial stabilization pair and compute destabilization	$O(g T )$	Theorem 4.7
DETECT REDUCTION	Find either a common component of $\alpha$ and $\beta$ or a separating curve disjoint from both	$O(\text{poly}(g, m,  T ))$	Theorem 4.8
DO A DEHN TWIST	Compute the action of a Dehn twist about a normal curve $s$ with complexity $m'$ on $\beta$	$O(((m + m') T )^{10})$	Theorem 4.9
GET $\pi_1$	Compute a presentation of the fundamental group of $M$ , with relations given by SLPs	$O(m T )$	Theorem 4.10
GET $H_1$	Compute a presentation of the first homology group of $M$	$\tilde{O}(m^2g^3 + m T )$	Theorem 4.12
GET $\beta_1$	Compute the first Betti number of $M$	$\tilde{O}(mg^3 + m T )$	Theorem 4.13

TABLE 1

**Theorem 4.4** (DO A PACHNER MOVE). *A diagram  $(T', E_{T'}(\alpha), N_{T'}(\beta))$ , where  $T'$  is the result of a Pachner move applied to any set of triangles in  $T$ , can be computed in time  $O(1)$ .*

*Proof.* Refer to the two moves of Figure 4. These modifications of the underlying are known as *Pachner moves* and have received special attention in low-dimensional topology because any two triangulations are related by finitely many applications of them [45]. Here, we assume that no such a move deletes an edge in  $E_T(\alpha)$ , otherwise, we would not have a marked triangulation as an output. Move  $(3, 1) \rightarrow (1, 3)$  corresponds to the simple deletion of the relevant components of  $N_T(\beta)$ , move  $(1, 3) \rightarrow (3, 1)$  involves adding new components whose values are corner coordinates. Both are implemented in time  $O(1)$  in our data structure for  $T$ . Similarly, moves  $(2, 2) \rightarrow (2, 2)$  can be implemented in time  $O(1)$  directly from computing the corner coordinates and updating the triangulation.  $\square$

**Theorem 4.5** (DO A DISK SLIDE). *A diagram  $(T, E_T(\alpha), N_T(\beta'))$ , where  $\beta'$  is the result of applying a disk slide on any two components of  $\beta$ , can be computed in time  $O(m|T|)$ .*

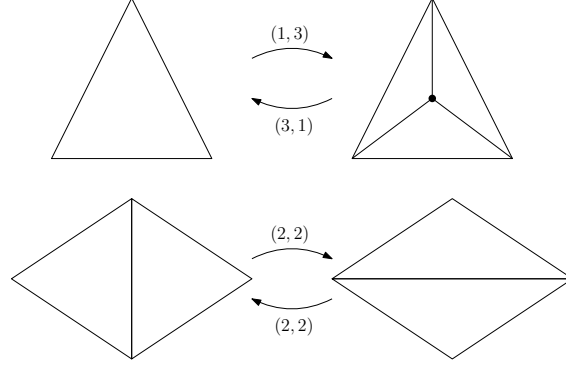


FIGURE 4

*Proof.* Compute the street complex  $S(T, \beta)$ , recall that it has complexity at most  $O(|T|)$ . Using breadth-first in the dual graph of  $S(T, \beta)$ , find, in time  $O(|T|^2)$ , the shortest arc  $p$  that connects faces adjacent to  $b_1$  and  $b_2$  and that does not cross any component of  $\beta$ , which can be avoided by adding infinite weights to the edges of  $S(T, \beta)$  not in  $T$ . Note that such an arc must exist because no component of  $\beta$  can be separating in the surface. Moreover, because  $p$  is shortest and therefore intersects at most  $O(|T|)$  streets in  $S(T, \beta)$ , we can compute using part (b) of Theorem 3.3, an SLP of complexity  $O(m|T| + |T|) = O(m|T|)$  of an intersection sequence of  $p$  with respect to  $T$ , call it  $I_T(p)$ .

Suppose that  $p$  is not trivial, that is, it is not only a single point. By Theorem 6.2 of [18], find, in time  $O(m|T|)$ , SLPs of the intersection sequences of  $b_1$  and  $b_2$  with respect to  $T$  starting at edges adjacent to the endpoint faces of  $p$ , call them  $I_T(b_1)$  and  $I_T(b_2)$ . Finally, let  $I_T(b) = I_T(b_2)^{-1} \circ I_T(p)^{-1} \circ I_T(b_1) \circ I_T(p)$ . Note that  $I_T(b)$  already is an intersection sequence of a normal curve in  $T$ . For, as  $p$  is a shortest path, it is normal in  $S(T, \beta)$ , which implies it is also normal in  $T$ . Moreover,  $p$  has as endpoints junctions in  $S(T, \beta)$  as, if it had streets as endpoints, there would be a shorter arc connecting  $b_1$  to  $b_2$  starting at one of the ends of the street. Therefore, any other reduction in  $I_T(b)$  would necessarily arise by  $p$  entering a junction of  $S(T, \beta)$  through a non-redundant port  $e$  that is also intersected by either  $b_1$  or  $b_2$ . But then, the other triangle in  $T$  adjacent to  $e$  is adjacent to either  $b_1$  or  $b_2$ , implying that  $p$  is not shortest. Part (c) of Lemma 2.2 finishes this case.

If  $p$  is trivial, then it means that  $b_1$  and  $b_2$  bound a same face in  $S(T, \beta)$ . Nonetheless, because the curves are not isotopic, there exists at least one face bounded by  $b_1$  and not bounded by  $b_2$ . We call such a face *good*. Choose, in time  $O(|T|)$ , one non-good face  $t_1$  that is adjacent to a good face through an edge  $e_1$ , see Figure 5. Note that  $e_1$  is the endpoint of a street  $s$  of sides in  $b_1$  and  $b_2$ . Look for the other end of this street,  $e_2$ —again, because  $b_1$  and  $b_2$  are not isotopic, the street has another end. Let  $t_2$  be the face (in fact, a junction) not equal to  $s$ , but also adjacent to  $e_2$ . Compute, once again through [18][Theorem 6.2], the sequence of faces adjacent to  $b_1$  starting at  $t_1$  and going all the way up to  $t_2$  without crossing  $s$ , call this sequence  $I_T(\tilde{b}_1)$ . Compute the related sequence for  $b_2$ , this time starting at  $t_2$ , call it  $I_T(\tilde{b}_2)$ . Let  $I_T(b) = I_T(\tilde{b}_2) \circ I_T(\tilde{b}_1)$ , note that it is also normal in  $T$  as  $b_1$  and  $b_2$  are normal and it enters  $t_1$  and  $t_2$  through distinct edges.  $\square$

**Theorem 4.6 (DO STABILIZATION).** *A diagram  $(T', E_{T'}(\alpha \cup \{a\}), N_{T'}(\beta \cup \{b\}))$  of a stabilization of  $(T, E_T(\alpha), N_T(\beta))$  can be computed in time  $O(1)$ .*

*Proof.* A similar algorithm for uncompressed intersection sequences as inputs is described in [16]; here we extend it to our data structure. First, let  $\gamma$  be a normal (multi)curve with respect to a triangulation  $T$ . Having fixed a triangle in  $T$ , we call its *corner coordinates* the number of elementary arcs of each type. In particular, note that for the triangle  $t$  with sides  $e$ ,  $f$ , and  $g$ , the

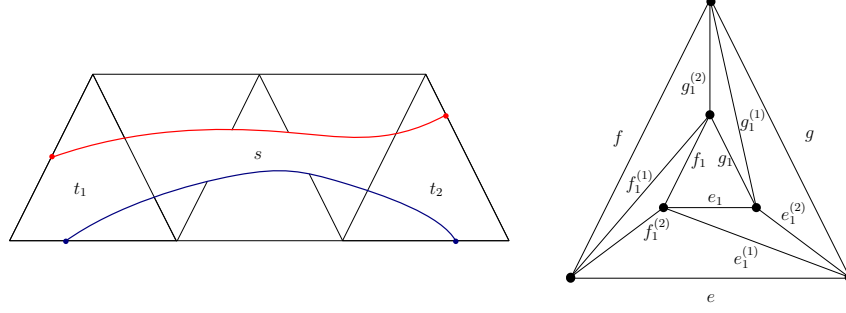


FIGURE 5. Left: diagram for the proof of Theorem 4.5. The red and blue curves represent  $b_1$  and  $b_2$ , the black lines are other edges of  $S(T, \beta)$ . The faces  $s$ ,  $t_1$ , and  $t_2$  are also indicated. Right: diagram for the proof of Theorem 4.6. Figure inspired by [16].

number of elementary arcs between sides  $e$  and  $f$  is  $1/2 \times [e(\gamma) + f(\gamma) - g(\gamma)]$  and symmetrically for the other cases. Given  $e(\gamma)$ ,  $f(\gamma)$ , and  $g(\gamma)$ , one can use these formulas to compute the corner coordinates in  $t$  in time  $O(1)$ .

Choose any such face  $t$  and modify it by adding a triangle  $t_1$  of sides  $e_1, f_1, g_1$  to its center, together with other 6 edges  $e_1^{(1)}, e_1^{(2)}, f_1^{(1)}, f_1^{(2)}, g_1^{(1)}, g_1^{(2)}$  connecting the vertices of  $t_1$  to the vertices of  $t$ , see Figure 5. Define the triangulation  $T_1$  as  $T$  with  $t_1$  deleted and update the normal coordinates of  $\beta$  to be a vector in  $\mathbb{N}^{|T|+9}$ , where the new components are set to

$$\begin{aligned} e_1(\beta), f_1(\beta), g_1(\beta) &\leftarrow 0 & e_1^{(1)}(\beta), e_1^{(2)}(\beta) &\leftarrow \frac{1}{2}[f(\beta) + g(\beta) - e(\beta)] \\ f_1^{(1)}(\beta), f_1^{(2)}(\beta) &\leftarrow \frac{1}{2}[g(\beta) + e(\beta) - f(\beta)] & g_1^{(1)}(\beta), g_1^{(2)}(\beta) &\leftarrow \frac{1}{2}[e(\beta) + f(\beta) - g(\beta)]. \end{aligned}$$

Note that  $T \setminus t_1$  is homeomorphic to  $\Sigma_g$  with one puncture.

Now let  $T_2$  be a fixed triangulation of the punctured torus with a triangular boundary component  $t_2$ , endowed with an edged curve  $a$  and a normal curve  $b$ , both disjoint from  $t_2$ . Glue  $T_1$  to  $T_2$  by identifying  $t_1$  with  $t_2$ . This forms a triangulation of  $\Sigma_{g+1}$ , with  $\alpha \cup \{a\}$  being an edged multicurve and  $\beta \cup \{b\}$  naturally giving a Heegaard diagram of a stabilization of  $(\Sigma_g, \alpha, \beta)$ .  $\square$

**Theorem 4.7 (DO DESTABILIZATION).** *One can find a trivial stabilization pair of the diagram  $(T, E_T(\alpha), N_T(\beta))$  in time  $O(g|T|)$  and, if found, a destabilization of the diagram can be computed in constant time.*

*Proof.* For each  $a \in \alpha$ , check the normal vectors of  $N_T(\beta)$ , in time  $O(g\|E_T(\alpha)\|)$ , for a  $a$  that intersects only a single component of  $\beta$  and only once. Suppose that there is such an  $a$  and that  $a, b$  is the detected trivial stabilization pair. In time  $O(\|E_T(a)\|) = O(|T|)$ , cut  $T$  at  $a$  and attach disks at the holes to have a triangulation of the surface of genus  $g - 1$ .  $\square$

**Theorem 4.8 (DETECT REDUCTION).** *There is an algorithm that runs in time  $O(\text{poly}(m, |T|))$  and detects whether a diagram is reducible. Moreover, if the diagram is reducible, it returns either an isotopic pair of  $a \in \alpha$  and  $b \in \beta$ , or a separating curve  $s$ .*

*Proof.* We divide the algorithm into two parts, corresponding to the two hypotheses of a reducibility of diagrams. For the first, apply [34][Theorem 6.3] to find, in polynomial time on the input, an isotopic diagram  $(\alpha, \beta')$  in efficient position where the complexity of  $\beta$  increases to  $m' = m(1+2|T|)$ . We note that although this subroutine is polynomial time on the input, the author of [34] does not provide an estimation of the polynomial degree and any attempt on our part to give one would be out of the scope of this paper. Because we made the diagram efficient, there can only be a component  $a \in \alpha$  isotopic to some  $b' \in \beta'$  if  $e(b') = 0$  for all  $e \in E_T(\alpha)$ . If that is the case, we trace  $S(T, b')$ . Since  $b' \cap a = \emptyset$ , the curve  $a$  is still fully in the edges of the street complex. Nonetheless,

$a$  is isotopic to  $b'$  if and only if they cobound a cylinder [19], a case that can be determined in time  $O(\|S(T, b')\|)$ . Checking this for every pair of curves  $a$  and  $b'$  that do not intersect gives a test for the first hypothesis.

If the above test returns no clear reduction pair, we look for a separating curve disjoint from  $\alpha$  and  $\beta$ . Trace  $S(T, \beta)$  and add infinite weight to the edges of the dual graph corresponding to crossings of  $E_{S(T, \beta)}(\beta)$ , therefore defining a cellular embedding for the  $2g$ -punctured sphere  $\Sigma_g \setminus \beta$ . In addition, for each street in  $E_{S(T, \beta)}(\beta)$ , we can determine in time  $O(\|E_T(\alpha)\| \times m|T|)$  with dynamic programming if there is an occurrence of an edge in  $E_T(\alpha)$  in the crossing sequence. Whenever that is the case, we also add infinite weights to the edges of the dual graph of  $E_{S(T, \beta)}(\beta)$  that cross the non-redundant ports bounding the street. Because each street is either a disk or a segment of an edge of  $T$ , adding the infinite weights defines a cellular embedding  $T'$  of a manifold homeomorphic to  $\Sigma' = \Sigma_g \setminus (\alpha \cup \beta)$ . We note that  $\Sigma'$  is a union of (potentially one) punctured spheres and that an essential separating curve exists if and only if all components are not disks. Assume that that is the case, then using the techniques of [17]—refer to Section 2.3 of [9] for details—one can compute, in time  $O(|T'|)$  an essential curve  $s$  in  $\Sigma_g \setminus (\alpha \cup \beta)$  expressed as an SLP of complexity  $O(m|T| + |T|) = O(m|T|)$ .  $\square$

**Theorem 4.9** (DO A DEHN TWIST). *Given a normal curve  $s$  in  $T$  of complexity  $\|N_T(s)\| = m'$ , there is an algorithm to compute, in time  $O(((m + m')|T|)^{10})$ , the diagram  $(T, E_T(\alpha), N_T(\tau_s(\beta)))$ .*

*Proof.* This algorithm is described by [49, 55]. If one requires only the intersection sequences  $I_T(\tau_s(\beta))$ , the algorithm can be executed in linear time on the inputs, but the output might just be standard with respect to the triangulation. Therefore, as in the proof of Theorem 3.6, we are forced to use the subroutines described by the same authors to cyclic reduce—either in time  $O(((m + m')|T|)^{10})$  with a deterministic algorithm or in time  $O(((m + m')|T|)^3)$  with a randomized one—the multicurve given by  $I_T(\tau_s(\beta))$ .  $\square$

**Theorem 4.10** (GET  $\pi_1(M)$ ). *A presentation of  $\pi_1(M)$  with the relations given by SLPs can be computed in time  $O(m|T|)$ .*

*Proof.* Referring to the discussion in the last paragraph of Section 2.1, one can find the fundamental group of  $M$  from the Heegaard diagram data. Formally, given  $I_T(\beta)$  delete, in linear time on the complexity of the SLPs, each reference of an edge  $E - E_T(\alpha)$  and substitute each edge of  $E_T(\alpha)$  by the symbol that represents its associated component, here seen as a generator  $\pi_1(M)$ . The total complexity is dictated by Theorem 3.3.  $\square$

**Remark 4.11.** In a sense, we report Theorem 4.10 for the sake of completion; we are unaware of whether presentations of 3-manifold groups [3] where the relations are given by SLPs have any applications. Nevertheless, we note that, for example, the four Tietze transformations [30] are easily implemented in, at most, linear time on the SLPs complexity.

**Theorem 4.12** (GET  $H_1(M)$ ). *The Smith normal form of the presentation matrix of  $H_1(M)$  can be computed in time  $\tilde{O}(m^2g^3 + m|T|)$ , where  $\tilde{O}$  indicates some hidden polylogarithmic factors.*

*Proof.* We first compute the presentation matrix  $K$  of the homology group, whose coefficients are algebraic intersection numbers between the diagram's curves. Because we assume that each  $a_j$  is a list of edges  $E_T(a_j)$ , given an SLP  $I_T(b_i)$ ,

$$\hat{i}(b_i, a_j) = \sum_{e \in E_T(a_j)} e(I_T(b_i)) - e^{-1}(I_T(b_i)),$$

which, by Lemma 2.2, can be computed in time  $O(\|I_T(b_i)\| \times \|E_T(a_j)\|)$ . Therefore, referring to Theorem 3.3 to compute  $I_T(\beta)$ , the total computational time of this procedure is  $O(m|T| +$

$\sum_{i=1}^g \sum_{j=1}^g \|I_T(b_i)\| \|E_T(a_j)\| \Big) = O(m|T| + m|T|)$ . Finally, for it to provide useful topological information, we need to reduce the matrix  $K$  to its Smith normal form. This can be achieved in time  $\tilde{O}(g^3 m^2)$  by the Kannan-Bachem algorithm [53].  $\square$

**Theorem 4.13** (GET  $\beta_1(M)$ ). *There is an algorithm to compute, in time  $\tilde{O}(mg^3 + m|T|)$ , the first Betti number  $\beta_1$  of  $M$ .*

*Proof.* Given the Smith normal form outputted by GET  $H_1$ , first Betti number can be computed in time  $O(g)$ . However, if the Betti number is the only homological information required, rational Gaussian elimination can be used to obtain it in time  $\tilde{O}(g^3 m)$  [4].  $\square$

## 5. EXAMPLES AND EXPERIMENTS

We here exemplify the usefulness of Heegaard diagrams by computing the homology group of manifolds in the so-called *random Heegaard splitting model* [3]. We say that the class of 3-manifolds is *asymptotically*  $\mathcal{P}$ , where  $\mathcal{P}$  is a property of 3-manifolds (e.g., hyperbolic, Haken, etc.), if for all  $g \geq 2$ , letting  $B(n) = \{\phi \in (\mathcal{L} \cup \mathcal{L}^{-1})^* \mid |\phi| = n\}$ ,

$$R = \lim_{n \rightarrow \infty} \frac{|\{\phi \in B(n) \mid (\Sigma_g, \phi(\alpha)) \text{ is } \mathcal{P}\}|}{|B(n)|} = 1.$$

Although it has been shown, for example, that manifolds are asymptotically hyperbolic [37, 38], rational homology spheres with torsion [14], and have particular probabilistic properties associated with some of their quantum invariants [15], other asymptotic properties, such as non-Hakeness and bounds on the hyperbolic volume [46], remain only conjectured.

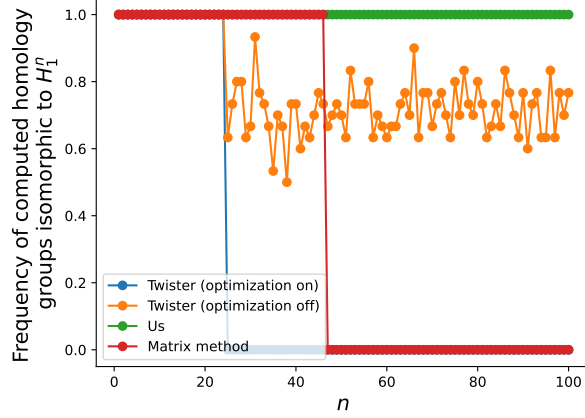
We might as well consider an *empirical* version of the random splitting model, in which we independently draw  $N$  words  $(\phi_i)_{i=1}^N \stackrel{\text{iid}}{\sim} \text{Uniform}(B(n))$  and consider the quantity

$$\hat{R}(n, N) = \frac{|\{\phi_i \mid (\Sigma_g, \phi_i(\alpha)) \text{ is } \mathcal{P}\}|}{N}.$$

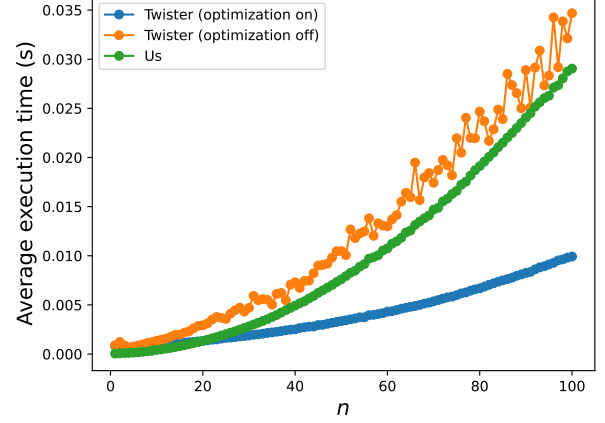
It is not hard to see that, as  $n, N \rightarrow \infty$ ,  $\hat{R}(n, N) \rightarrow R$ , meaning that the empirical model can be useful to explore some of the open questions regarding random splittings. Interestingly, however, to the best of our knowledge, there is a notable lack of studies which profit from this approach, with the few exceptions, such as [46], computing properties related to  $\hat{R}(n, N)$  by first triangulating Heegaard splittings with the **Twister** module [5] of **SnapPy** [11] and then using algorithms for triangulations to find relevant quantities. In some instances, such as for homology-dependent properties, the appeal to triangulations, nonetheless, not only adds computational cost but also seems to introduce some numerical instability, as we show in this section.

Here, we contrast **Twister** with a combination of the algorithm of Theorem 3.6 and GET  $H_1$  (Theorem 4.12) to compute homology groups. Because the input of the experiments consists of Heegaard words, we note that there is no need to use proper normal coordinates or even triangulations of  $\Sigma_g$ ; instead, we might compute the SLPs of the induced diagram with respect to general cellular embeddings, therefore avoiding the high cost of cyclic reductions.

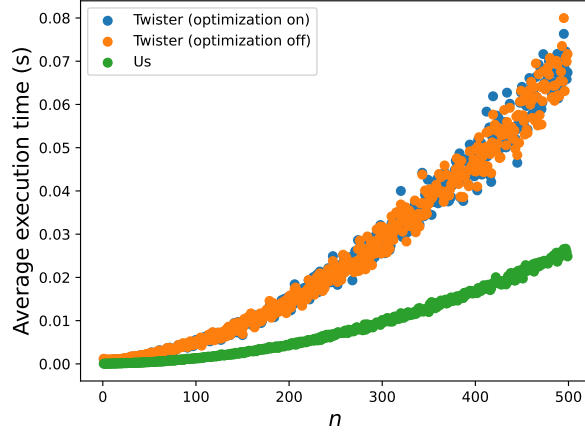
**5.1. Genus 1.** Heegaard splittings over the torus are worth discussing not only because they yield a well-studied family of 3-manifolds, the *lens spaces*, but also because of the classical modular representation of  $\text{Mod}(\Sigma_1)$  in  $\text{SL}(\mathbb{Z}^2)$  [19, 47], which allows for some correctness benchmarks to be traced. Explicitly, any Heegaard splitting  $(T^2, a, b)$  can be expressed through a vector in  $(p, q) \in \mathbb{Z}^2$ , where  $p$  represents the number of signed intersections of  $b$  and the usual longitude of the torus,  $\ell$ , and  $q$  the signed intersections with the canonical meridian,  $a$ . Under this notation, Dehn twists about the meridian and longitude can be described by linear maps  $(p, q) \mapsto (p, q-p)$  and  $(p, q) \mapsto (p+q, q)$ , respectively, and the homology group of  $(T^2, a, \phi(a))$  can be computed by  $O(|\phi|)$ -many  $2 \times 2$  matrix



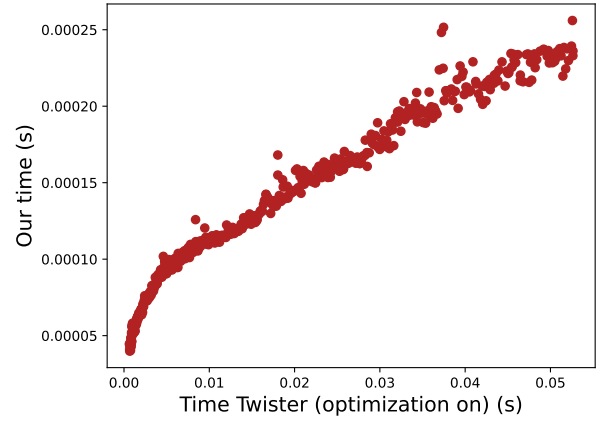
(A) Frequency of agreement of the computed homology groups  $H_1(T^2, a, \phi_n(a))$  with  $H_1^n$  for distinct methods.



(B) Average time of different methods to compute  $H_1((T^2, a, \phi_n(a)))$ .



(C) Average time of different methods to compute  $H_1((T^2, a, \psi_n(a)))$  for  $(\psi_i)_{i=1}^N \stackrel{\text{iid}}{\sim} \text{Uniform}(B(n))$ .



(D) **Twister's** (with optimization) average computational time of the homology group  $H_1$  of the family  $(T^2, a, \tau_\ell^n(a))$  versus our method's.

FIGURE 6. Experiments with computing the homology group  $H_1$  of Heegaard splittings over the torus. Frequencies and averages were computed for 30 repetitions.

multiplications and a constant-time coordinate query, yielding an approach that we call the *matrix method*. In particular, direct recursion on the matrix method implies that homology group of the splitting of word  $\phi_n = (\tau_a^{-1} \circ \tau_\ell)^n$  equals  $H_1^n = \mathbb{Z}/f_{2n}$ , where  $f_n$  is the  $n$ -th entry of the Fibonacci sequence starting at zero.

In Figure 6a, the computed homology groups of the manifold  $(T^2, a, \phi_n(a))$  through **Twister** (with and without optimization, where by *optimization* the authors mean greedily folding of tetrahedra in the construction of a triangulation of  $(\Sigma_g, a, \phi(a))$ , refer to their documentation<sup>2</sup> for details) and the matrix method, implemented using **numpy**, are compared to the actual values  $H_1^n$ , computed from the Fibonacci sequences. These two methods are to be contrasted with ours. The experiments are repeated 30 times for each value of  $n$  to capture instabilities of **SnapPy's** subroutines on the computation of  $H_1$ . The figure indicates the frequency which the homology groups computed are isomorphic to the expected  $H_1^n$ . Although all methods agree with the ground-truth

<sup>2</sup>Available at <https://snappy.computop.org>.



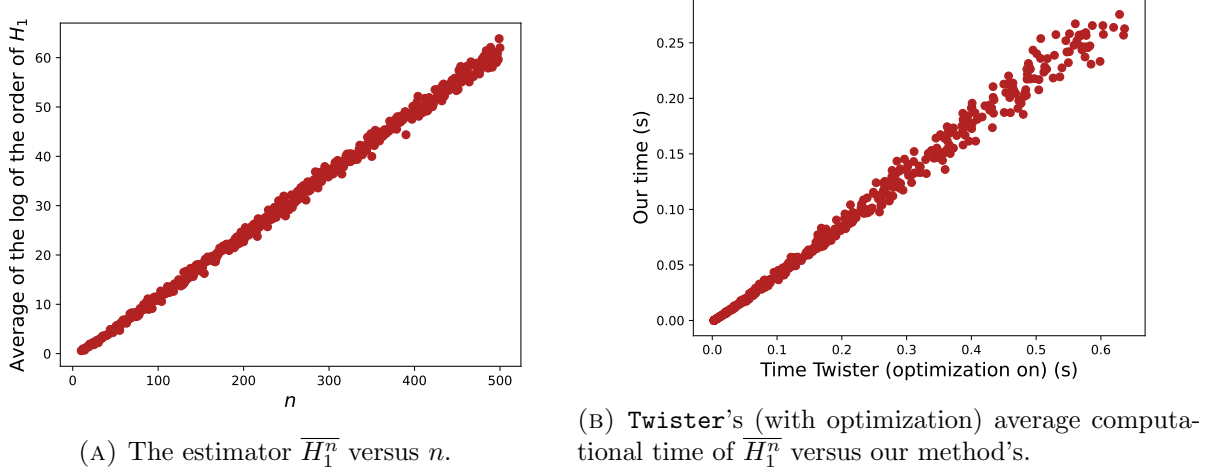


FIGURE 7. Experiments with computing the estimator  $\overline{H_1^n}$  for Heegaard splittings over the torus. Averages were computed for 30 repetitions.

homology  $H_1^n$  for short sequences, when  $n \geq 25$ , **Twister's** output is not always isomorphic to the expected group, while **numpy** deviates only after  $n = 47$ . The lack of numerical robustness of these techniques might be traced to their reliance on rather unstable matrix manipulations, while our method, whose computed homology agrees with  $H_1^n$  for all investigated values of  $n$  (our method also agrees with  $H_1^n$  for up to  $n = 500$ , the maximum value we tested), uses only simple integer operations and therefore seems preferable for this problem.

In terms of computational time, our technique is slightly slower than **Twister**, as can be seen in Figure 6b. Nevertheless, it is worth highlighting that, while the latter is partially implemented in **C++**, ours is fully in **python**. However, we often have significant gains over **Twister** in the general case, as shown in Figure 6c, where we compare the average time to compute the first homology group of closed 3-manifolds defined by independently drawing random Heegaard words  $(\psi_n)_{i=1}^N \stackrel{\text{iid}}{\sim} \text{Uniform}(B(n))$  with  $n$  now varying from 1 to 500. The speed-ups in computational time arise from simplifying repeated occurrences of Dehn twists in  $\psi_n$  to power notation as in Theorem 3.6. While  $\tau_s^k$  can be computed in time  $\lg k$  (provided  $k$  is given in binary) by our techniques, by triangulating Heegaard words with the current algorithms, one is forced to represent the manifold with at least  $O(|\tau_s^k|) = O(k)$ -many tetrahedra (before folding), meaning that the more repetitions in  $\psi_n$ , the greater is our gain with respect to **Twister**. This is stressed in Figure 6d, where our computational time is compared to **Twister's** (with optimization) for the family  $(T^2, a, \tau_\ell^n(a))$ . There is some clear gain in our case: while the total complexity of **Twister** seems to be  $O(n^c)$  for some  $c > 1$ , ours is only  $O(n + \lg n) = O(n)$ . What is more, if we allow inputs *already* in power-notation form, we can easily construct families of 3-manifolds for which the computation of their homology groups would require exponential time through **Twister**, but can be done in linear time in our framework.

**Remark 5.1.** In fact, if we restrict the analysis to the very well-behaved *layered triangulations* [29], a triangulation of the lens space has a minimal of  $\sum_i (a_i) - 1$  tetrahedra, where  $(a_0, \dots, a_k)$  is the continued fraction expansion of  $q/p$  (with  $q$  and  $p$  as defined for the matrix method). In particular, provided that we work solely with layered triangulations, we have a theoretical guarantee that  $(T^2, a, \psi_{2^n}(a))$  defines an infinite family of 3-manifolds that can be represented with Heegaard diagrams of complexity  $n$ , but with a triangulation of size at least  $2^n$ .

**5.2. Genus 2.** For the case of Heegaard splittings over the double torus, no faithful representation of  $\text{Mod}(\Sigma_2)$  is known, which means that we lack more effective methods to check the correct

convergence of the homology computations. This time, however, we have that the random Heegaard splitting model asymptotically gives rational homology spheres with torsion [14], that is, of zero Betti number, but with  $H_1$  finite. In particular, [46] shows that the random variable  $\overline{H_1^n} = \frac{1}{n} \sum_{i=1}^N \log |H_1((\Sigma_g, \psi_n^i(\alpha)))|$  where  $(\psi_n)_{i=1}^N \stackrel{\text{iid}}{\sim} \text{Uniform}(B(n))$  follows a Central Limit Theorem

$$(5.2) \quad \frac{1}{\sqrt{N}}(\overline{H_1^n} - n\lambda) \rightarrow \mathcal{N}(0, \sigma^2)$$

for some positive constants  $\sigma$  and  $\lambda$ , as  $N \rightarrow \infty$  (restricted to cases where  $\log |H_1((\Sigma_g, \psi_n^i(\alpha)))|$  is finite). Equation (5.2) can be used as in Figure 7a to test the validity of our computations of the homology groups. In particular, we estimate the coefficient  $\lambda$  as 0.13. For the genus 2 case, **Twister**'s results and ours were this time identical for all experiments, but we were, once again, consistently faster in the average case, as indicated in Figure 7b.

**Remark 5.3.** For  $g = 2$ , the homology groups of the manifolds  $(\Sigma_g, \alpha, \psi_n(\alpha))$  estimated by **Twister** and our methods agreed up to  $n = 1000$ , which includes groups of order significantly superior to the orders that both methods started to deviate in the  $g = 1$  case. This implies that the inconsistencies described in Section 5.1 are likely not due to some difference in the maximum integer storable in the implementation of **Twister** and ours, as one might be inclined to suppose. Moreover, to guarantee that the errors did not arise from the subroutines where we computed Smith normal forms—which are used in the case of  $g = 2$ , but unnecessary for lens spaces—we experimented with different implementations of the Kannan-Bachem algorithm, namely **sympy**'s [41] and **SNF**'s [40], all which were consistent with **SnapPy**'s implementation. The lower robustness of **Twister** in computing the homology of lens spaces and its behavior for  $g > 2$  remains therefore to be investigated.

## REFERENCES

- [1] Gorjan Alagic and Edgar A. Bering. Quantum algorithms for invariants of triangulated manifolds. *Quant. Inf. Comput.*, 12(9-10):0843–0863, 2012. [1]
- [2] Gorjan Alagic and Catharine Lo. Quantum invariants of 3-manifolds and NP vs #P. *Quantum Info. Comput.*, 17(1-2):125–146, February 2017. [1]
- [3] M. Aschenbrenner, S. Friedl, and H. Wilton. *3-manifold Groups*. EMS series of lectures in mathematics. European Mathematical Society, 2015. [4, 14, 15]
- [4] Erwin H Bareiss. Sylvester's identity and multistep integer-preserving gaussian elimination. *Mathematics of computation*, 22(103):565–578, 1968. [15]
- [5] Mark Bell, Tracy Hall, and Saul Schleimer. Twister (computer software). [https://bitbucket.org/Mark\\_Bell/twister/](https://bitbucket.org/Mark_Bell/twister/), 2008–2014. Version 2.4.1. [1, 15]
- [6] Benjamin A Burton. Efficient enumeration of 3-manifold triangulations. *AUSTRALIAN MATHEMATICAL SOCIETY GAZETTE*, 31(2):108–114, 2004. [1]
- [7] Benjamin A Burton. A new approach to crushing 3-manifold triangulations. In *Proceedings of the twenty-ninth annual symposium on Computational geometry*, pages 415–424, 2013. [1]
- [8] Benjamin A. Burton, Ryan Budney, William Pettersson, et al. Regina: Software for low-dimensional topology. <http://regina-normal.github.io/>, 1999–2023. [1]
- [9] Erin W Chambers, Éric Colin De Verdière, Jeff Erickson, Francis Lazarus, and Kim Whittlesey. Splitting (complicated) surfaces is hard. In *Proceedings of the twenty-second annual symposium on Computational geometry*, pages 421–429, 2006. [14]
- [10] Francesco Costantino, Yang-Hui He, Elli Heyes, and Edward Hirst. Learning 3-manifold triangulations. *Journal of Physics A: Mathematical and Theoretical*, 2024. [1]
- [11] Marc Culler, Nathan M. Dunfield, Matthias Goerner, and Jeffrey R. Weeks. SnapPy, a computer program for studying the geometry and topology of 3-manifolds. Available at <http://snappy.computop.org> (19/05/2025). [1, 15]
- [12] Basudeb Datta. Minimal triangulations of manifolds. *arXiv preprint math/0701735*, 2007. [1]
- [13] Olivier Devillers, Jean-Daniel Boissonnat, Mariette Yvinec, and Monique Teillaud. Triangulations in cgal. In *Proceedings of the 16th Annual Symposium on Computational Geometry*, pages 11–18. ACM, 2000. [5]
- [14] Nathan M Dunfield and William P Thurston. Finite covers of random 3-manifolds. *Inventiones mathematicae*, 166:457–521, 2006. [15, 18]

- [15] Nathan M Dunfield and Helen Wong. Quantum invariants of random 3-manifolds. *Algebraic & Geometric Topology*, 11(4):2191–2205, 2011. [15]
- [16] Henrique Ennes and Clément Maria. Hardness of computation of quantum invariants on 3-manifolds with restricted topology, 2025. [1, 3, 12, 13, 20]
- [17] Jeff Erickson and Sarel Har-Peled. Optimally cutting a surface into a disk. In *Proceedings of the eighteenth annual symposium on Computational geometry*, pages 244–253, 2002. [7, 10, 14]
- [18] Jeff Erickson and Amir Nayyeri. Tracing compressed curves in triangulated surfaces. *Discrete Computational Geometry*, 49(4):823–863, June 2013. [2, 6, 8, 10, 12]
- [19] Benson Farb and Dan Margalit. *A primer on mapping class groups*, volume 41. Princeton University Press, 2011. [2, 14, 15]
- [20] Torben Hagerup. Sorting and searching on the word ram. In *STACS 98: 15th Annual Symposium on Theoretical Aspects of Computer Science Paris, France, February 25–27, 1998 Proceedings 15*, pages 366–398. Springer, 1998. [2]
- [21] Wolfgang Haken. Über das homöomorphieproblem der 3-mannigfaltigkeiten. i. *Mathematische Zeitschrift*, 80(1):89–120, 1962. [1]
- [22] Allen Hatcher. *Algebraic Topology*. Cambridge University Press, 2002. [4, 7, 8, 21]
- [23] Allen Hatcher and William Thurston. A presentation for the mapping class group of a closed orientable surface. *Topology*, 19(3):221–237, 1980. [21]
- [24] Alexander He, James Morgan, and Em K Thompson. An algorithm to construct one-vertex triangulations of Heegaard splittings. *arXiv preprint arXiv:2312.17556*, 2023. [7]
- [25] John Hempel. 3-manifolds as viewed from the curve complex. *Topology*, 40(3):631–657, 2001. [3, 20]
- [26] John Hempel. *3-Manifolds*, volume 349. American Mathematical Society, 2022. [4]
- [27] William Jaco and Ulrich Oertel. An algorithm to decide if a 3-manifold is a haken manifold. *Topology*, 23(2):195–209, 1984. [1]
- [28] William Jaco and J Hyam Rubinstein. 0-efficient triangulations of 3-manifolds. *Journal of Differential Geometry*, 65(1):61–168, 2003. [1]
- [29] William Jaco and J Hyam Rubinstein. Layered-triangulations of 3-manifolds. *arXiv preprint math/0603601*, 2006. [1, 17]
- [30] David Lawrence Johnson. *Presentations of groups*. Number 15. Cambridge university press, 1997. [14]
- [31] Jesse Johnson. Notes on heegaard splittings. *preprint*, 2006. [2, 3, 4, 20]
- [32] Greg Kuperberg. Identifying lens spaces in polynomial time. *Algebraic & Geometric Topology*, 18(2):767–778, 2018. [1]
- [33] Marc Lackenby. Algorithms in 3-manifold theory, 2020. [1]
- [34] Marc Lackenby. Some fast algorithms for curves in surfaces. *arXiv preprint arXiv:2401.16056*, 2024. [2, 10, 13]
- [35] Marc Lackenby and Jessica S Purcell. The triangulation complexity of elliptic and sol 3-manifolds. *Mathematische Annalen*, 390(2):1623–1667, 2024. [1]
- [36] William BR Lickorish. A finite set of generators for the homeotopy group of a 2-manifold. In *Mathematical Proceedings of the Cambridge Philosophical Society*, volume 60, pages 769–778. Cambridge University Press, 1964. [3]
- [37] Alexander Lubotzky, Joseph Maher, and Conan Wu. Random methods in 3-manifold theory. *Proceedings of the Steklov Institute of Mathematics*, 292:118–142, 2016. [15]
- [38] Joseph Maher. Random heegaard splittings. *Journal of Topology*, 3(4):997–1025, 2010. [15]
- [39] Sergei Vladimirovich Matveev and SV Matveev. *Algorithmic topology and classification of 3-manifolds*, volume 9. Springer, 2007. [1, 7]
- [40] Corbin McNeill. Smith Normal Form (SNF). GitHub repository, 2025. <https://github.com/corbinmcneill/SNF>. [18]
- [41] Aaron Meurer, Christopher P Smith, Mateusz Paprocki, Ondřej Čertík, Sergey B Kirpichev, Matthew Rocklin, AMiT Kumar, Sergiu Ivanov, Jason K Moore, Sartaj Singh, et al. Sympy: symbolic computing in python. *PeerJ Computer Science*, 3:e103, 2017. [18]
- [42] Masamichi Miyazaki, Ayumi Shinohara, and Masayuki Takeda. An improved pattern matching algorithm for strings in terms of straight-line programs. In *Combinatorial Pattern Matching: 8th Annual Symposium, CPM 97 Aarhus, Denmark, June 30–July 2, 1997 Proceedings 8*, pages 1–11. Springer, 1997. [10]
- [43] Edwin E Moise. Affine structures in 3-manifolds: V. the triangulation theorem and hauptvermutung. *Annals of mathematics*, 56(1):96–114, 1952. [3]
- [44] Harriet Handel Moser. Upper bound on distance in the pants complex. *Journal of Homotopy and Related Structures*, 9(2):495–511, 2014. [21]
- [45] Udo Pachner. Pl homeomorphic manifolds are equivalent by elementary shellings. *European journal of Combinatorics*, 12(2):129–145, 1991. [11]

- [46] Igor Rivin. Statistics of random 3-manifolds occasionally fibering over the circle. *arXiv preprint arXiv:1401.5736*, 2014. [15, 18]
- [47] Nikolai Saveliev. *Lectures on the topology of 3-manifolds: an introduction to the Casson invariant*. Walter de Gruyter, 2011. [3, 15]
- [48] Marcus Schaefer, Eric Sedgwick, and Daniel Štefankovič. Algorithms for normal curves and surfaces. In *Computing and Combinatorics: 8th Annual International Conference, COCOON 2002 Singapore, August 15–17, 2002 Proceedings 8*, pages 370–380. Springer, 2002. [2, 6]
- [49] Marcus Schaefer, Eric Sedgwick, and Daniel Štefanković. Computing Dehn twists and geometric intersection numbers in polynomial time. In *CCCG*, volume 20, pages 111–114, 2008. [2, 5, 14]
- [50] Saul Schleimer. Notes on the complex of curves. *unpublished notes*, 2006. [20]
- [51] Saul Schleimer. Sphere recognition lies in np. *Low-dimensional and symplectic topology*, 82:183–213, 2011. [1]
- [52] Jennifer Schultens. *Introduction to 3-manifolds*, volume 151. American Mathematical Soc., 2014. [2, 4]
- [53] Francis Sergeraert. About the kannan-bachem algorithm, 2024. [15]
- [54] Isadore Manuel Singer and John A Thorpe. *Lecture notes on elementary topology and geometry*. Springer, 2015. [2]
- [55] Daniel Štefankovič. *Algorithms for simple curves on surfaces, string graphs, and crossing numbers*. Phd thesis, University of Chicago, 2005. Available at <http://people.cs.uchicago.edu/~laci/students/stefankovic-phd.pdf>. [2, 8, 14]
- [56] Michael Yoshizawa. High distance heegaard splittings via dehn twists. *Algebraic & Geometric Topology*, 14(2):979–1004, 2014. [3, 20]

## APPENDIX A. EXTENSION TO GENERAL SYSTEMS

As mentioned in Remark 2.1, there is a generalization that allows systems to have more than  $g$  components. In particular, for this section, we will assume that a *system* is a multicurve of cardinality at least  $g$  and with no isotopic components. A standard Euler characteristic argument [50] implies that a system  $\gamma$  cuts  $\Sigma_g$  into  $\#\gamma - g + 1$  at least thrice punctured spheres. When  $\#\gamma = g$ , we say that the system is *minimal* and it reduces to the definition used in the main text. If, on the other hand,  $\#\gamma = 3g - 3$ , we say that the system is *maximal* or a *pants decomposition* because it cuts  $\Sigma_g$  into a union of three-times punctured spheres known as *pairs of pants*.

Like minimal systems, general systems uniquely define handlebodies. This means that the notion of equivalence naturally extends to the more general systems, even if they have different cardinality. In particular, one [16, 31] can show that, provided that  $\gamma$  is not a pants decomposition, the band sum  $c$  of two punctures  $c_1$  and  $c_2$  and an arc  $p$  connecting them in  $\Sigma_g \setminus \gamma$  is a meridian of  $\mathcal{H}_\gamma$  and is not isotopic to any other component of  $\gamma$ . This means that  $\gamma' = \gamma \cup \{c\}$  forms a system which is equivalent to  $\gamma$ ; we call  $\gamma'$  an *extension* of  $\gamma$ .

We can expand our data structure to allow for more general systems for  $\alpha$  and  $\beta$ . In particular, a diagram  $(\Sigma_g, \alpha, \beta)$  is *minimal* if  $\alpha$  and  $\beta$  are minimal systems; similarly it is *maximal* if they are pants decomposition. In fact, although more resource-intensive, this general version of Heegaard diagrams has been used both in mathematical (for example, [25, 56]) and in computer science ([16]) settings. All algorithms described in this paper can be adapted to this more general notion of Heegaard diagrams with only minor modifications. We can, moreover, describe efficient methods to translate between minimal and more general systems. This is exactly the content of the next two results.

**Theorem A.1 (REDUCE TO MINIMAL).** *Let  $(T, E_T(\alpha), N_T(\beta))$  be a Heegaard diagram of complexity  $m$ . Then one can compute an equivalent minimal Heegaard diagram  $(T, E_T(\alpha'), N_T(\beta'))$  in time  $O(m|T|)$ .*

*Proof.* Compute  $S(T, \beta)$  and delete the separating components of  $\beta$  by using breadth-first in the dual graph. In total, this takes time  $O(m|T| + g|T|) = O(m|T|)$  since  $O(g) = O(|T|) = O(\sqrt{m})$ . Similarly, delete separating curves in  $\alpha$  in time  $O(g|T|)$ .  $\square$

**Theorem A.2 (EXTEND TO MAXIMAL).** *Let  $(T', E_{T'}(\alpha), N_{T'}(\beta))$  be a Heegaard diagram of complexity  $m$ . Then one can compute an equivalent maximal Heegaard diagram  $(T, E_T(\alpha'), N_T(\beta'))$  in time  $O(gm|T|)$ .*

*Proof.* Without loss of generality, suppose  $(T, E_T(\alpha), E_T(\beta))$  is a minimal diagram; we want to extend each multicurve to a pants decomposition. Both cases can be treated similarly thanks to the following lemma.

**Lemma A.3.** *Suppose  $\gamma$  is an edged minimal system in a cellular embedding  $T$  of a surface  $\Sigma_g$ . Then one can find a pants decomposition  $\gamma'$ , equivalent to  $\gamma$ , in time  $O(g|T|)$ .*

*Proof.* Note that  $\Sigma_g \setminus \gamma$  is homomorphic to the  $2g$  punctured sphere, so let  $d_1, \dots, d_{2g}$  represent the boundary components of this surface. We will find some  $2g-3$  new separating curves  $d_{2g+1}, \dots, d_{3g-3}$  in  $\Sigma_g$  that recursively define pairs of pants as follows. In step  $i$ , choose a curve  $d_{g+j}$ ,  $0 \leq j \leq i-1$  from a list of available curves. Call this choice  $s_1$  and pick a face  $t$  adjacent to  $s_1$ . Using breadth-first search, we find, in time  $O(|T|)$ , the shortest path  $p$  in the dual graph starting from  $t$  to any face adjacent to one of the available curves. Call the closest available curve  $s_2$  and remove  $s_1$  and  $s_2$  from the list of available curves. Note that we can encode  $p$  as a list of faces of  $T$ . In time  $O(\|E_T(s_1)\|) = O(|T|)$ , we update  $p$  by iteratively removing all faces adjacent to  $s_1$  except for the last one. By construction,  $p$  intersects each edge of the cellular complex at most once and does not intersect any face adjacent to an available curve, except for exactly one face adjacent to  $E_T(s_1)$  and one face adjacent to  $E_T(s_2)$ .

As in the proof of Theorem 4.5, make  $I_T(d_i) = I_T(s_2)^{-1} \circ I_T(p)^{-1} \circ I_T(s_1) \circ I_T(p)$ , where  $p$  is potentially trivial, and add  $d_i$  to the list of available curves. The curve  $d_i$  separates a thrice puncture sphere component with punctures defined by  $s_1$ ,  $s_2$ , and  $d_i$ , from a  $2g-i$  punctured sphere component, and which component is which can be identified in time  $O(|T|)$ . We then update  $T$  to a cellular embedding of  $\Sigma_0^{2g+i}$  by adding the edges and vertices defined by  $I_T(d_i)$  to the graph and blocking paths in the dual graph transverse to them. While  $T$  becomes more complicated at each step, because the arc  $p$  is constructed to intersect a constant number of faces adjacent to the available curves and the curves  $d_{g+j}$ ,  $1 \leq j \leq i-1$ , are separating, at each step, breadth-first needs only to consider  $O(|T|)$  many edges and vertices of the dual graph of  $T$ . The algorithm terminates when  $i = 3g-3$ , in which case we have defined, by construction, a maximal system  $\gamma = \{c_1, \dots, c_g, d_{g+1}, \dots, d_{3g-3}\}$ .  $\square$

We now apply Lemma A.3 to get some pants decomposition equivalent to  $\alpha$ , edged in a new triangulation  $T'$ . Because  $|T'| = O(|T|)$ , we can use the discussion of corner coordinates to find the coordinates  $N_{T'}(\beta)$  in time  $O(g|T|)$ . We then compute some edged pants decomposition equivalent to  $\beta$  in  $S(T', \beta)$ . Finally, by the very proof of Lemma A.3 and part (b) of Theorem 3.3, this gives the normal coordinates of the new  $\beta$  curves with respect to  $T'$ .  $\square$

**Remark A.4.** Theorem A.2 *does not* guarantee that there exists a  $\phi \in \text{Mod}(\Sigma_g)$  such that  $\beta' = \phi(\alpha')$  where  $\alpha'$  and  $\beta'$  are pants decompositions. In fact, it is a well-known result from surface theory [44] that such a homeomorphism exists if and only if the *pants decomposition graphs* associated with  $\alpha'$  and  $\beta'$  are isotopic. One can easily imagine a modification to the algorithm of the theorem that constructs a pants decomposition  $\beta'$  that defines a graph isotopic to the graph defined by  $\alpha'$  by forcing arcs between particular punctures of  $\Sigma_g \setminus \alpha'$  as in Theorem 4.5, but that would imply an algorithm exponential on  $|T|$ . Alternatively, a method based on the Hatcher and Thurston proof of connectivity of the *pants graph* (not to be confused with the pants decomposition graph) [23][Appendix] can be devised, but efficiency in  $g$  is not trivial.

## APPENDIX B. DETAILS ON THE IMPLEMENTATIONS OF SECTION 5

As mentioned in the main text, several simplifying assumptions were made for the implementation of the examples in Section 5. First and most importantly, we *did not* compute a data structure for the Heegaard diagrams as described in Section 3. Instead, we use general cellular embedding  $T_g$  given by the fundamental polygons of  $\Sigma_g$  [22] to represent the surfaces, which implies that, instead of normal coordinates, we assumed the  $\beta$  curves to be given by SLPs  $I_T(\beta)$ . Although

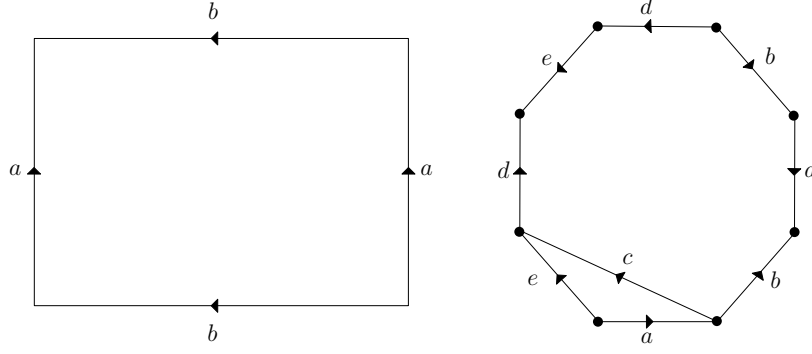


FIGURE 8. The cellular embeddings  $T_g$  for  $g = 1$  (left) and  $g = 2$  (right) with the choices of edge labels agreeing with **Twister**.

this deviates from what was described in this paper, we note that cyclic reducing the SLPs is irrelevant to finding  $H_1(M)$  and introduces some unbearable computational cost. We also assumed the Lickorish generators to be edged with respect to  $T_g$  and that their intersection sequences are computed only once, say as a preprocessing step, using Lemma 3.5 (in fact, for these experiments, we computed the SLPs by hand). Figure 8 shows  $T_g$ , for  $g = 1$  and 2, while Table 2 indicates the edged and (uncompressed) intersection sequences of the curves involved.

Genus	$E_{T_g}(\alpha)$	$I_{T_g}(\alpha)$	$E_{T_g}(\mathcal{L})$	$I_{T_g}(\mathcal{L})$
$g = 1$	$[a]$	$b$	$[b]$	$a^{-1}$
$g = 2$	$[a]$ $[e]$	$b$ $d^{-1}$	$[b]$ $[c]$ $[d]$	$c^{-1} \cdot a$ $b \cdot d$ $c^{-1} \cdot e^{-1}$

TABLE 2. Here, we use  $[\cdot]$  to denote lists. We assume that the  $\alpha$  curves are contained in the Lickorish generators, meaning that they are omitted in the fourth and fifth columns.